MACRAMÉ

Deliverable Report D2.7

Report on Performances of High-Resolution Imaging for the Quantification of AdMAs

Project & Programme Information	
Project Acronym	MACRAMÉ
Project Full Name	Advanced Characterisation Methodologies to assess and predict the Health and Environmental Risks of Advanced Materials
Grant Agreement No.	101092686
Work Programme	HORIZON.2.4 - Digital, Industry and Space
Call and Topic Name	HORIZON-CL4-2022-DIGITAL-EMERGING-01-35 - Advanced characterisation methodologies to assess and predict the health and environmental risks of nanomaterials
Instrument	Horizon Europe – Research and Innovation Action (RIA)
Project Start Date	01 December 2022
Duration	36 months

Disclaimer

The information in this document is as provided and no guarantee or warranty is given that the information is fit for any particular purpose.

This document reflects only the author's view and the European Commission is not responsible for any use that may be made of the information it contains.

MACRAMÉ has received funding from:
the European Union's Horizon Europ
Research and innovation programm
under grant agreement No. 1010926

Schweizerische Eidgenossenschaft
Confédération suisse
Confederazione Svizzera
Confederaziun svizra

Swiss Confederation

Federal Department of Economic Affairs,
Education and Research EAER
State Secretariat for Education,
Research and Innovation SERI

UKRI Innovate UK

Deliverable Report Information	
Work Package	WP2 - Development and Advancement of Characterisation- & Test-Methods &-Protocols
Deliverable Number	D2.7 - Report on Performances of High-Resolution Imaging methods for the Quantification AdMa@CMs
Associated Task	Task 2.4: Development of high-resolution Imaging Methods for the Quantification of AdMas in Cells and Tissues
Type [1]	R
Dissemination Level [2]	SEN
Version	V1.0
Actual Submission Date	16/10/2025
Contractual Submission Date	30/09/2025
Lead author (organisation)	Martin Wiemann (IBE)
Contributors	Martin Wiemann (IBE), Antje Vennemann (IBE), Alexander Köhrer (BASF), Daniel Breitenstein (Tascon), Francine Wang (LNE), Maike Stange (BAuA)
Reviewers	Steffi Friedrichs (AIST), Daniel Breitenstein /Tascon), Alexander Köhrer (BASF), Maike Stange (BAuA)

[1] R= Document, report (excluding the periodic and final reports); DEM = Demonstrator, pilot, prototype, plan designs; DEC = Websites, patents filing, press & media actions, videos, etc.; DATA =Data sets, microdata, etc.; DMP = Data management plan; ETHICS = Deliverables related to ethics issues; SECURITY = Deliverables related to security issues; OTHER = Software, technical diagram, algorithms, models, etc.

[2] PU = Public, fully open, e.g. web (Deliverables flagged as public will be automatically published in CORDIS project's page); SEN = Sensitive, limited under the conditions of the Grant Agreement; Classified R-UE/EU-R = EU RESTRICTED under the Commission Decision No2015/444; Classified C-UE/EU-C = EU CONFIDENTIAL under the Commission Decision No2015/444; Classified S-UE/EU-S = EU SECRET under the Commission Decision No2015/444

MACRAMÉ has received funding from:
the European Union's Horizon Euro
Research and innovation programm
under grant agreement No. 101092
Schweizerische Eidgenossenschaft
Confédération suisse
Confederazione Svizzera
Confederaziun svizra
Swiss Confederation
Federal Department of Economic Affairs, Education and Research EAER
State Secretariat for Education, Research and Innovation SERI
UKRI Innovate UK

Version	Date	Changes made	By	Sent to	Purpose
0.1	01.08.2025	Draft version	Antje Vennemann	Martin Wiemann (IBE R&D gGmbH)	Partner contribution
0.2	11.08.2025	Contribution	Daniel Breitenstein (Tascon)	Antje Vennemann (IBE R&D gGmbH)	Partner contribution
0.3	13.08.2025	Contribution	Francine Wang (LNE)	Antje Vennemann (IBE R&D gGmbH)	Partner contribution
0.4	14.8.2025	Contribution	Alexander Köhrer (BASF)	Antje Vennemann (IBE R&D gGmbH)	Partner Contribution
0.5	16.9.2025	Contribution	Maike Stange (BAuA)	Antje Vennemann (IBE R&D gGmbH)	Partner Contribution
0.6	22.9.2025	Updated Draft version	Antje Vennemann	Martin Wiemann (IBE R&D gGmbH) and google drive	Review
0.7	26.09.2025	Update	Martin Wiemann	Steffi Friedrich (AIST)	Review
0.8	30.09.2025	Update	Martin Wiemann	Steffi Friedrich (AIST)	Finalisation
1.0	16.10.2025	Finalisation	Steffi Friedrichs (AIST)	European Commission	Submission

MACRAMÉ has received funding from:
the European Union's Horizon Euro
Research and innovation programm
under grant agreement No. 101092
Schweizerische Eidgenossenschaft
Confédération suisse
Confederazione Svizzera
Confederaziun svizra
Swiss Confederation
Federal Department of Economic Affairs, Education and Research EAER
State Secretariat for Education, Research and Innovation SERI
UKRI Innovate UK

Acronyms Listed in this Document	
AdMas	Advanced Material
ALI	Air Liquid Interface
AMA	Alveolar Macrophage Assay
Au	Aurum = Gold
CaF	Calcium Fluoride
CLS	Classical Least Squares
CRM	Confocal Raman Microscopy
EC	European Commission
eDFM	Enhanced Darkfield Microscopy
fg	Femtogram
FLG	Few Layer Graphene
FP	Frustrated Phagocytosis
FW	Fibre Winding
FWHM	Full Width at Half Maximum
GO	Graphene Oxide
GR2DM	Graphene Related 2D Material
h	Hour
HCD	Higher-energy Collisional Dissociation
IDA	Isotope Dilution Analysis
LA-ICP-MS	Laser Ablation - Inductively Coupled Plasma - Mass Spectrometry
mL	Millilitre
MML	MACRAMÉ's material Library
MWCNT	Multi Walled carbon Nanotube
NM	Nanomaterial
NP	Nanoparticle
NPL	National Physical Laboratory
P	Phosphor
PLGA	Poly(lactid-co-glycolid)
PSU/PU	Polysulfone/Polyurethane
PVP	Polyvinylpyrrolidon

Acronyms Listed in this Document	
ROI	Region of Interest
Sc ICP-MS	Single Cell Inductively Coupled Plasma - Mass Spectrometry
SEM	Scanning Electron Microscopy
SiC	Silicon Carbide
SOP	Standard Operating Procedure
te	Ttarget element
TE	Transport Efficiency
ToF-SIMS	Time-of-Flight Secondary Ion Mass Spectrometry
UC	Use Case
WP	Work Package
µg	Microgram
µl	Microlitre
µm	Micrometre
3D	Three dimensional

Content

1 Introduction - High-Resolution Imaging Methods 13
2 Confocal Raman Microscopy 13
2.1 SOP Development for Confocal Raman Microscopy 14
2.2 UC1: Identifying Graphene Oxide Flakes in Incinerated and Wastewater Samples by using SEM and Confocal Raman Microscopy 16
2.3 UC2: Raman 3D-Image Scan from Graphene Flakes in Epoxy Plates 17
2.4 UC2: Detection of Few Layer Graphene in Cells by Confocal Raman Microscopy 17
2.5 UC3: Detection and Characterisation of Graphene from Spray Material by Confocal Raman Microscopy 18
2.6 Correlative Imaging of MWCNT NM-401 in NR8383 Cells by Confocal Raman Microscopy and Scanning Electron Microscopy 20
3 ToF-SIMS Analyses 21
3.1 Method Development for Correlative ToF-SIMS Measurements 22
3.2 Detection of FLG by ToF-SIMS and Confocal Raman Microscopy 24
3.3 Correlative Imaging of PLGA in NR8383 Cells by ToF-SIMS and Fluorescence Microscopy 25
4 Time-Lapse Video Microscopy 27
4.1 Time-Lapse Video Microscopy of NR8383 Cells with SiC and NM-401 28
4.2 Time-Lapse Video Microscopy of NR8383 Cells with Graphene Oxide Material 29
5 Enhanced Darkfield Microscopy 31
6 Quantitative LA-ICP-MS 32
6.1 Method Development 33
6.2 Quantification Method 33
6.3 Ablation Techniques for Single-Cell LA-ICP-MS 34
6.4 Data Evaluation 35
6.5 Application of the Developed Automated Method 37
6.6 Quantitative Single Cell ICP-MS 39
7 Conclusions 41
8 Bibliography 42

Table of Figures

Figure 1: Representative Raman spectra (left) and examples of corresponding brightfield images (right) of Raman measurements on flakes of JRG graphene (JRC NM 48001a) and Carbon Waters Few Layer Graphene (FLG) taken at IBE R&D gGmbH (A) and BAuA (B). Raman spectra were acquired with 532nm laser, 1 mW and 1-3 sec acquisition time on 300 flakes, averaged and background corrected. The peaks were Lorentzian fitted by the software and the calculated results are shown in Table 2. 15

Figure 2: Brightfield image of the filter after the Fibre Winding (FW) process water and Raman intensity image (A) and merged images (B); SEM image of a FW water sample filter (C) and the Raman signal of GO (D), orange arrows pointing to the GO flakes. 16

Figure 3: Three-dimensional reconstruction of the FLG distribution inside FLG-epoxy, the starting material of UC2. The confocal Raman image stack, prepared from 30 mappings taken down to a depth of 30 µm, reveals the heterogeneous size of the FLG, accounting for approximately 5% of the total mass. 17

Figure 4: Results of the Confocal Raman Microscopy (CRM) of macrophages incubated with a dispersion of Few Layer Graphene (FLG) for 16 h. (A) Reflected light microscopy reveals various black inclusions in the cytoplasm outside the central, nuclear region. (B) Region selected from (A) for Raman mapping. (C) Raman spectrum with characteristic D-, G-, and 2D-bands Raman bands identifying the black material as FLG according to Table 1. (D) Raman mapping of the area in (B); the spatial distribution of the G-band, as highlighted in (C), is shown in red. 18

Figure 5: Results of Raman microscopy of a NR8383 macrophage incubated with the settled dark fraction prepared from UC3 Spray "Graphene+Silicone". (A) Darkfield and brightfield microscopy (B) show light scattering and dark material, respectively, seemingly located in the nuclear region, which had been artificially caused by centrifugation. Raman mapping reveals characteristic graphene-related bands (C). By CLS fitting (D) the spatial distribution of Raman bands corresponding to DNA (cell nucleus), cytoplasm, and GRM are displayed. E: Transmission electron microscopy image of a GRM-loaded NR8383 cell (Epon embedded, unstained 60 nm thick section). A large GRM agglomerate is seen in an electron-lucent, structureless area pointing to an artificial re-assembly after sectioning. The structure is located in the cytoplasm close to the nucleus; small and large arrows point to electron lucent and electron dense portions, respectively, representing different numbers of graphene layers... 19

Figure 6: Comparative measurements of a "100% Graphene Spray" UC3 material with Raman microscopy at IBE and BAuA. (A) shows the sprayed material settled on CaF carriers which (upper, GR2M) contains large dark agglomerations of the graphene-related 2D material in question. The lower panels show oily drops (additive(s)) partially containing the dark material as well. (B) shows representative Raman spectra from the dark material (upper, GR2M) which was identified as graphene-related, and from the additive which was identified as to be paraffin by BAuA. Note that all spectra measured by IBE and BAuA were highly consistent. 20

Figure 7: Correlative Imaging of a NR8383 macrophage treated with multiwalled carbon-nanotubes (MWCNT NM-401, 22.5 µg/ml). (A) 3D reconstruction of the Raman z-stack mapping showing the cell (green) and a multiwalled carbon-nanotube (red) protruding from the cell. (B) Corresponding Raman spectra with typical Raman bands of MWCNT NM-401 (red line) and cellular constituents (green line). (C) SEM image of the same cell found after automatically retracing the position. (D) Brightfield microscopy of the same cell (transmitted light mode); dark lines in the cell indicate MWCNT NM-401; arrows in (C) and (D) pointing at the same fibre structure. (Scale box in (A) in µm; all other scale bars show 5µm) 21

Figure 8: SIMS Spectra on pure graphene oxide material. Under the conditions shown here, numerous signals specific for graphene oxide were detected. Their typical composition is C_{2n}^+ while minor detergent contamination was detected. However, under the conditions optimised for cell imaging the number of signals are significantly decreased, e.g. as high mass components to not survive extensive primary ion bombardment that has to be used in SIMS-imaging. 22

Figure 9: Comparison of a microscopic image (left), the image acquired with the camera of the ToF-SIMS instrument (bottom), and the ToF-SIMS image (right) of macrophages exposed to Carbon Black. In the ToF-SIMS image, carbon-specific signals are shown in green, phosphate signals in red, and the cell-specific CN^- signal in blue. 23

Figure 10: Comparison of images obtained by Raman microscopy (left), light microscopy (centre), and ToF-SIMS imaging (right) of the same individual macrophage loaded with Carbon Black. Carbon-specific signals are shown in green in both the Raman and ToF-SIMS images. In the ToF-SIMS image, the phosphate signal is displayed in red, while the cell-specific CN^- signal is shown in blue. 24

Figure 11: Correlative Raman and ToF-SIMS measurement of a FLG-loaded cell. (A) Bright field overview image of FLG-loaded NR8383 cells spun on a gridded coverslip with a cyto-centrifuge for Raman and ToF-SIMS measurements. (B) Higher magnification of the cell boxed in (A) showing several discrete dark spots; Laser position of the Raman measurement shown in (C) is indicated by the green cross. (C) Raman spectrum from the dark agglomerate marked in (B); characteristic D, G and 2D bands are typical for FLG. (D) ToF-SIMS imaging of the same macrophage; carbon-specific signals are shown in green, phosphate signal of the nucleus is displayed in red, and the protein-specific CN^- signal of the cell is shown in blue. 24

Figure 12: SIMS MS/MS fragmentation of Lumogen. This fluorphore was detected in PLGA particles and its fragmentation pattern was extensively studied under increasing Normalised Collision Energies (NCE): any detected signal is one fragment of the Lumogen molecule and the respective sum formula was assigned. 25

Figure 13: Lumogen containing PLGA particles analysed by Secondary Ion Mass Spectrometry. The analysis results in a comparatively complex but regular fragmentation pattern of the polymeric material. Beside polymer specific fragments also other materials like fatty acids and polysiloxane could be detected. 26

Figure 14: Comparison of ToF-SIMS imaging (left) and fluorescence microscopy (right) of macrophages exposed to PLGA particles loaded with the fluorophore Lumogen. Top row: After 2 hours of incubation, both the fluorophore (fluorescence microscopy) and the polymer (ToF-SIMS) show a similar, co-localised distribution. Bottom row: After 20 hours, the fluorophore signal is in some cells confined to specific intracellular regions (likely lysosomes), while the polymer remains widely distributed throughout the cell. 27

Figure 15: Time-Lapse Video Microscopy of a NR8383 alveolar macrophage in the process of frustrated phagocytosis with several SiC fibres. Indicated times t0 – t6 correspond to images taken up to 6 hours after fibres had been added to the culture. 28

Figure 16: Time-Lapse Video Microscopy of NR8383 alveolar macrophages in contact with NM-401, a multiwalled carbon nanotube material. NM-401 was dispersed following the NanoGenotox protocol and administered with a concentration of 11.25 µg/mL. Indicated times t0 – t6 correspond to images taken up to 6 hours after fibres had been added to the culture. Unlike the situation with SiC (see Figure 15) the process here is less clear as only some fibre agglomerates are very long. However, successive images show that the cell is not capable of

bending and/or completely ingesting the agglomerated fibre bundle, strongly suggesting that NM-401 at least in agglomerated form, gives rise to frustrated phagocytosis. 29

Figure 17: Time-Lapse Video Microscopy of NR8383 alveolar macrophages in contact with graphene oxide, dispersed following the Empa protocol (45 min water bath sonication) and administered with a concentration of 11.25 mg/mL. Indicated times t0 – t6 correspond to images taken up to 10 hours after fibres had been added to the culture. Cells were unable to ingest the large black particles (diameter approximately 20 µm) to which they appear to adhere. 30

Figure 18: Time-Lapse Video Microscopy of NR8383 alveolar macrophages in contact with incinerated graphene oxide, dispersed following the Empa protocol (45 min water bath sonication) and administered with a concentration of 11.25 mg/mL. Indicated times t0 – t6 correspond to images taken up to 10 hours after fibres had been added to the culture. Cells were freely moving and ingested all soot particles, the largest of which were below 5 µm. . 30

Figure 19: Brightfield (graphene, MWCNT NM-401, and SiC NW) and enhanced Darkfield Microscopy (SiO_2 NM-203, quartz DQ12) of Pappenheim-stained cytospin preparations of NR8383 cells. Note that the cells are differentially loaded with the material which relates to the LA-ICP-MS measurements of single cells (see above). 31

Figure 20: Enhanced Darkfield-Microscopy (eDFM) of NR8383 macrophages to analyse the uptake of Au-doped PLGA (UC5). Cytospin preparations of Pappenheim-stained cells. Gold-nanoparticle (Au-NP) used for PLGA labelling had a diameter of 50 nm. (A) control cells with few light scattering objects. (B) Cells loaded with 5 µg/mL of the original Au-NP (as used to prepare PLGA-Au); the arrow points to a heavily loaded cell with light scattering inclusions. (C) Same as (B) but with a concentration of only 0.05 µg/mL to match the gold concentration of the diluted PLGA preparation in D (calculation of concentration based on the PLGA-Au data sheet). Virtually no light-scattering Au-NP are seen inside cells. (D) Cells subjected to a non-toxic PLGA preparation (dilution factor: 500); the cytoplasm contains no bright but numerous pale bright inclusions, interpreted as PLGA containing endocytotic vesicles devoid of gold labelling. Since a higher concentration of PLGA-Au proofed to by cytotoxic no attempts were made to intensify the Au-PLGA loading for LA-ICP-MS investigation. 32

Figure 21: Results of calibration experiments. Mean intracellular Ce concentrations of n = 100 NR8383 cells incubated under varying conditions were determined using liquid, microdroplet, and IDA-based calibrations. Error bars indicate standard errors of the mean. 34

Figure 22: Schematic of different ablation modes. (a) One spot is used for the entire cell. (b) The cell is ablated line by line, distributing the signal over multiple pixels. 35

Figure 23: Visualisation of the three phosphorous-based cell recognition algorithms as used for automated evaluation. NR8383 cells were loaded with 22.5 µg/mL Mn_2O_3 for 16 h, detached from the cell culture well, suspended, and spin-dried onto a glass slide with a Cyto-centrifuge. The size of the scanned area was 500 µm x 2600 µm. Red lines indicate demarcate single cell regions as recognised by (a) the simple approach, (b) the geometric approach, and (c) the verbose approach. 36

Figure 24: Flaws of the geometric approach. (a) Zoomed-in sector of Figure 18 showing inaccurate cell allocation. (b) Comparison of median pixel numbers "per cell" as obtained from the three approaches; data were taken from all experiments carried out to detect Mn, Ce, Co, and W (see experiments listed in Table 3). 37

Figure 25: Boxplots of mass uptake distribution in all incubation experiments with different NMs determined with the optimised LA-ICP-MS method. Values after data evaluation with the

simple (blue) and the verbose (green) algorithm of cell identification are shown. Median and mean values are indicated by a solid and a dashed line inside boxes, respectively. Boxes represent the range between 25th and 75th percentile (Q1/Q3), whiskers show Q1-1.5·IQR and Q3+1.5·IQR (interquartile range). 38

Figure 26: Gold mass distribution in PVP-coated Au-NPs suspended in PBS (in orange) and in A549 cells loaded with PVP-coated AuNPs (in green). The dashed line corresponds to the 99.9th percentile of PVP-coated Au-NPs suspended in PBS. Both samples were suspended in PBS. 40

Table of Tables

Table 1: Peak intensity ratios ID/IG and I2D/IG to characterise the number of graphene layers. 14

Table 2: Characterisation results of Raman measurements on Carbon Waters few layer graphene (FLG) flakes and JRC graphene (JRC NM 48001a) flakes obtained at IBE R&D gGmbH and BAuA by averaging spectra from more than 300 flakes each and Lorentzian fitting. 15

Table 3: Particles and concentrations from MACRAMÉ's particle library as used for loading and preparation of NR8383 cells for LA-ICP-MS experiments. 37

Executive Summary

Assessing the toxicological effects of particles with in vitro cell models requires the careful description of particle uptake. Because cells may differ in their ability to ingest and concentrate particles to which they were subjected, High-Resolution Imaging is the method of choice to visualise and quantify particle distribution in any type of cell culture. In MACRAMÉ, state of the art imaging tools were employed not only to detect but also to chemically identify particulate matter inside cells, as this would be a main task for unknown samples. This Deliverable is the outcome of Task 2.4 and describes the development and adaptation of various optical and analytical imaging methods for the detection and quantification of Advanced Materials (AdMas) from both, MACRAMÉ's Use Cases 1 - 5 (UC 1-5) and MACRAMÉ's Materials Library (MML).

The identification and detection of the various carbon-based materials was a challenging task mainly solved with Confocal Raman Microscopy (CRM) in combination with other microscopic techniques. Graphene from JRC (from MML) and the Few Layer Graphene (FLG, from UC2) were detected in cells by CRM plus light and electron microscopy using the SOPs from D2.2. FLG in an Epoxy matrix (a material from UC2) was also detected in a semi-quantitative fashion using 3D reconstruction of image stacks. A graphene material included in a lubricant spray (a material from UC3) was identified by CRM as to be graphite- rather than graphene-like when investigated both, outside and inside cells; electron microscopy of the loaded cells then revealed a partially condensed, partially lamellar and more graphene-like morphology possibly explaining the CRM results. Concerning the uptake of multi-walled carbon nanotubes (NM-401, from MML) by macrophages a correlative approach of CRM and scanning electron microscopy (SEM) not only identified the carbon fibres but showed them to be incompletely phagocytised. This finding relates to the so-called frustrated phagocytosis, a key event for the carcinogenicity of such materials. All these examples underpin the necessity to combine different analytical methods for identifying and localizing carbonaceous AdMas in organic matrices.

Time-of-Flight Secondary Ion Mass Spectrometry (ToF-SIMS), as a destructive, label-free, High-Resolution Imaging technology, was employed to study various AdMas in macrophages. Prior to analysis, the cells were inspected with light and/or fluorescence microscopy to define adequate regions of interest. This generated additional images which were used for correlative approaches, as in the case for fluorescent PLGA (UC5 material). Here, the distribution of the fluorescent marker and the PLGA matrix were clearly different, providing new insights into the intracellular dynamics of medical PLGA particles in cells. The ToF-SIMS methodology was furthermore refined for the detection of carbonaceous materials such as Carbon Black (from MML), graphene oxide (from UC1) or FLG (from UC2) inside cells. Again, these images were combined with light microscopic and CRM images. The multitude of analyses show that Tof-SIMS is a valuable technique to detect AdMas of known composition in an organic matrix.

Enhanced Darkfield Microscopy (eDFM) allows the visualisation of small light scattering objects. In MACRAMÉ eDFM was used to detect gold (Au) nanoparticles, Au-doped PLGA, as well as transparent amorphous or crystalline silica (NM-203, quartz DQ12, both from MML) all of which were not detectable by conventional light microscopy. Time-lapse video microscopy was used for visualizing the fibre uptake by macrophages (NM-401, SiC, both from MML). Both light microscopic approaches complemented the images obtained with CRM and Tof-SIMS described above.

A quantitative High-Resolution Imaging was conducted with Laser Ablation - Inductively Coupled Plasma - Mass Spectrometry (LA-ICP-MS). To this end, particle-loaded alveolar macrophages were provided on glass slides as air-dried specimens, using a cytospin centrifuge. Particle loading of the cells matched the procedure used for the Round Robin, which was

conducted to validate the alveolar macrophage assay (as part of WP2.3). Here, CeO_2, Cobalt-doped Tungsten Carbide (Co-WC), and Mn_2O_3 (all from MML) were chosen as analytes. Based on the cells' phosphorus signal, an automated cell recognition algorithm was developed, which allowed to attribute the quantified analytes to single cells. While the results were partially biased by some destruction of heavily loaded cells during the cytospin preparation, the method allows to quantify low amounts of cell associated AdMas, if the respective elements are accessible to LA-ICP-MS detection. Another ICP-MS-based approach, the single cell ICP-MS, was impaired by the disruption of Au-loaded cells being injected into the ICP. Preliminary data nevertheless confirm the uptake of fg amounts of Au.

Overall, the work carried out in this Deliverable has shown that a quantitative High-Resolution Imaging of AdMas in cells is possible within certain limits set by the cell model and the detectability of the material. Considerable progress has been made in detecting and identifying carbonaceous materials in single cells and organic matrices, although the quantification of these materials requires further development.

1 Introduction - High-Resolution Imaging Methods

The detection of Advanced Materials (AdMas) in cells is a decisive prerequisite for the sound interpretation of in vitro testing results. Considering the heterogeneous culture systems used in MACRAMÉ to represent different parts of the lung, especially phagocytic cells tend to ingest materials, whereas e.g. epithelial cells have no or limited particle uptake capacities but nevertheless may contact materials. Other cell systems such as MucilAir or EpithelAir (from Epihelix) form mucus or surfactant layers on top, partially shielding cells underneath against particles administered as suspensions or aerosols from above. Exploring the inhomogeneities in particle distribution of such cultures requires High-Resolution Imaging methods at least at the cellular level.

Methods such as Confocal Raman Microscopy (CRM) allow combining spectroscopic analyses for the identification of submicron-sized inclusions with light and electron microscopy. With respect to the carbonaceous materials investigated in MACRAMÉ, CRM proved to be a valuable tool for the semi-quantitative detection of AdMas within biological and other matrices. Correlative approaches were also possible with Time-of-Flight Secondary Ion Mass spectrometry (Tof-SIMS), another high- resolution technique, together with sophisticated light microscopic techniques such as fluorescence microscopy or enhanced Darkfield Microscopy (eDFM). While all the aforementioned techniques can deliver semi-quantitative imaging data on the particle distribution in cells, Laser Ablation – Inductively Coupled Plasma – Mass Spectrometry (LA-ICP-MS) is a quantitative imaging method, applicable to detect most elements except for those with low mass numbers (H, He, C, N, O), halogens (F, Cl), and some others. LA-ICP-MS allows for cellular resolution and is applicable to cells and tissue sections on glass slides. For cells in suspension, single cell Inductively Coupled Plasma – Mass Spectrometry (sc ICP-MS) may be used.

In the next chapters we will provide selected examples of how MACRAMÉ's Use Cases and Library materials were imaged.

2 Confocal Raman Microscopy

Confocal Raman Microscopy (CRM) is a micro-spectroscopic method and the gold standard for determining the vibrational modes of molecules. Its main use in unknown micro-samples is to provide a structural fingerprint, which is how molecules can be identified.

Raman scattering is the basic mechanism and known to be based on the inelastic scattering of photons. Monochromatic light of a laser interacts with molecular vibrations, phonons, or other excitations in the system, whereby energy is transferred from either the photons to the molecule resulting in a downshift in energy of the photon. Or energy is donated to the photon by the molecule and enhances the photon's energy. The shift in energy is shown as a shift in the frequency and is called Stokes shift.

This excitation results in the molecule entering a virtual energy state for a brief period before a photon is emitted. Inelastic scattering refers to the phenomenon whereby the energy of the emitted photon is either lower or higher than that of the incident photon. Following the scattering event, the sample is found to be in a different rotational or vibrational state. The specific composition of energy shifts shown in a spectrum can be used as a fingerprint for identifying a molecule in a mixture of components in a matrix [1].

2.1 SOP Development for Confocal Raman Microscopy

IBE and BAuA both conducted CRM studies on the MACRAMÉ materials but used different instruments. To make the Raman measurements from both institutes highly comparable, a common SOP was developed so that Raman measurements on 2D carbon-based materials became standardised. This allowed e.g. the standardised measurements of Graphene-related materials with respect to purity, number of graphene layers, and distribution in samples. The SOP development was based on the Good Practice Guide: Characterisation of the Structure of Graphene from NPL[2].

The resulting SOP 'Raman measurement for characterisation of graphene-related advanced materials - Characterisation of 2D carbon materials' is part of the Deliverable D2.2 (see MACRAMÉ File Exchange platform) and became an important basis of Task 2.4. It may be recalled from D2.2 that the following parameters from Raman spectra (see also Figure 1 for illustration) are key to the identification of carbon materials:

- Peak intensity ratio for the G- and 2D-peaks: I2D/IG
- Peak intensity ratio for the D- and G-peaks: ID/IG
- Full Width at Half Maximum for the D-peak: FWHM(D)
- Full Width at Half Maximum for the 2D-peak: FWHM(2D)
- peak position D (cm-1)
- peak position G (cm-1)
- peak position 2D (cm-1)

For example, the peak intensity ratios ID/IG and I2D/IG may be used to estimate the number of layers for a given graphene material, as shown in Table 1.

Table 1: Peak intensity ratios ID/IG and I2D/IG to characterise the number of graphene layers.

parameter	single layer graphene	double layer graphene	few layer graphene	multi layer graphene
I_D/I_G	≈ 0	≈ 0.05	≈ 0.1	≥ 0.15
I_{2D}/I_G	≈ 2	≈ 1	≈ 0.8	≤ 0.5

These values provide information on the characteristics of the material and on the quality of their suitability for Raman measurements. As shown in Figure 1 and Table 2, values from BAuA and IBE for two materials (Carbon Waters FLG, JRC graphene) were highly similar.

Based on these results, further analyses of Use Case materials were conducted and are shown in the chapters below.

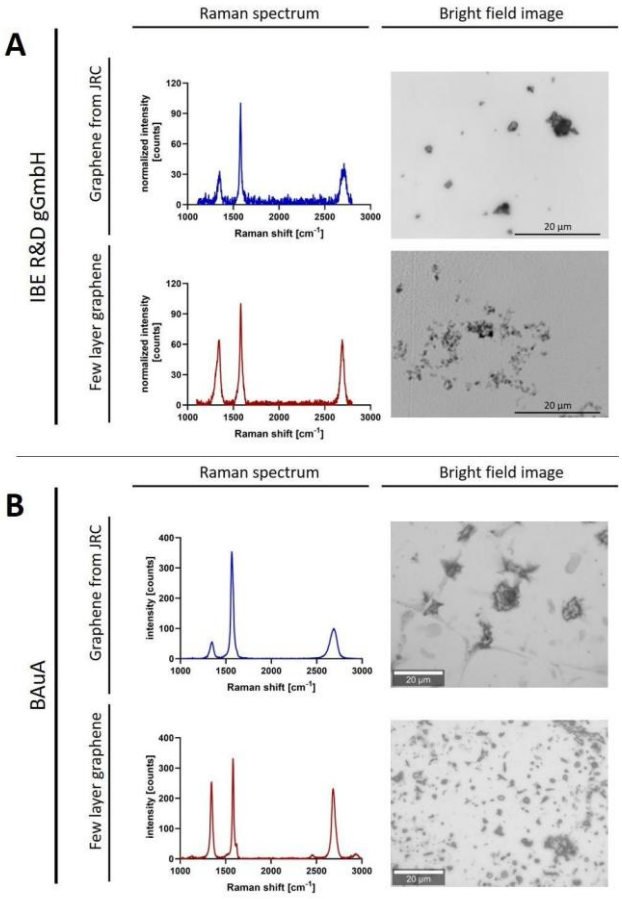


Figure 1: Representative Raman spectra (left) and examples of corresponding brightfield images (right) of Raman measurements on flakes of JRG graphene (JRC NM 48001a) and Carbon Waters Few Layer Graphene (FLG) taken at IBE R&D gGmbH (A) and BAuA (B). Raman spectra were acquired with 532nm laser, 1 mW and 1-3 sec acquisition time on 300 flakes, averaged and background corrected. The peaks were Lorentzian fitted by the software and the calculated results are shown in Table 2.

Table 2: Characterisation results of Raman measurements on Carbon Waters few layer graphene (FLG) flakes and JRC graphene (JRC NM 48001a) flakes obtained at IBE R&D gGmbH and BAuA by averaging spectra from more than 300 flakes each and Lorentzian fitting.

characterisation parameter	Carbon Waters FLG		JRC graphene	
	BAuA	IBE	BAuA	IBE
FWHM(D)	23	33	32	34.8
FWHM(2D)	32	46	51	56.3
I_D/I_G	0.78	0.66	0.16	0.27
I_{2D}/I_G	0.72	0.69	0.31	0.28
peak position D (cm^{-1})	1344	1343	1345	1346
peak position G (cm^{-1})	1582	1579	1568	1577
peak position 2D (cm^{-1})	2687	2689	2684	2702

2.2 UC1: Identifying Graphene Oxide Flakes in Incinerated and Wastewater Samples by using SEM and Confocal Raman Microscopy

Raman spectroscopy was applied to analyse the materials used in a water filter and to monitor their release throughout the product's life cycle. The filter consists of an acrylonitrile butadiene styrene (ABS) cage, a polyurethane (PU) cap, and graphene oxide (GO)-containing polysulfone (PSU) fibres. Reference spectra from pristine materials were used for identification, and on polycarbonate filters incinerated samples were examined to detect residues from combustion. Additionally, process water from three manufacturing stages was analysed: blank process water (BPW) at the inlet, fibre winding (FW) process water, and static fibre washing (SFW) water. GO flakes in powder form served as a further reference.

Characteristic Raman peaks for GO appeared at 1344 and 1602 cm^{-1}, consistent with low-reduced graphene oxide, alongside broad overlapping peaks at 2704, 2929, and 3187 cm^{-1}. PSU and PU materials were identified by distinct spectral features matching reference data, and ABS was confirmed through strong peaks and additional detection of a nacre-coloured pigment. No specific Raman signals of ABS or PU were detected in incinerated residues on Si-wafer or copper tape, while GO signals were potentially obscured by amorphous and defective carbon in soot. Consequently, incinerated materials were dissolved in isopropanol and examined by scanning electron microscopy (SEM) to search for remaining GO flakes or PSU residues.

SEM analysis of nanopore filters with 50 nm pore size revealed no detectable GO flakes in BPW. However, GO was clearly released into process water during the FW step. No GO flakes were detected in the SFW water, even at very high magnifications, suggesting no significant release at this stage.

In summary, the combined Raman and SEM analyses provided detailed identification of filter materials and demonstrated that GO release occurs primarily during the fibre winding process but is not detectable during subsequent washing or in incinerated material. Overall, this correlative approach turned out to be a valuable tool for the life cycle analysis of AdMas.

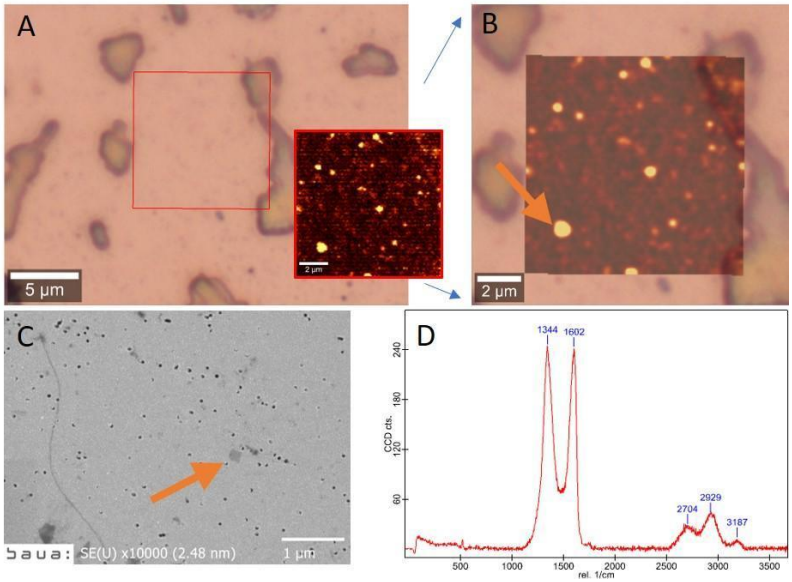


Figure 2: Brightfield image of the filter after the Fibre Winding (FW) process water and Raman intensity image (A) and merged images (B); SEM image of a FW water sample filter (C) and the Raman signal of GO (D), orange arrows pointing to the GO flakes.

2.3 UC2: Raman 3D-Image Scan from Graphene Flakes in Epoxy Plates

MACRAMÉ's focus on carbon-based AdMas was a challenge for detecting, characterising and quantifying such materials within different matrices. Raman microscopy provided a versatile tool to identify carbon-based AdMas in many different matrices such that product relevant polymers, as well as biological and environmental matrices could be handled to supplement toxicity and ecotoxicity studies with data on cellular uptake and tissue distribution.

UC2 consisted of Epoxy plates doped with Few Layer graphene (Epoxy-FLG) which were converted to particles by taber abrasion. Non-doped epoxy and pure few layer graphene (FLG) as well as the incinerated material (i.e. soot particles prepared from the original Epoxy-FLG plates) were included for comparison. All these materials were subjected to CRM to follow the uptake of material into cells and to describe possible changes of FLG Raman signals.

Although Raman mapping is not a quantitative technique per se, it may be used in a semi-quantitative manner. One example is the characterisation of the UC2 materials, for which a three-dimensional map of the FLG distribution inside the epoxy matrix was prepared. Figure 3 shows an example selected for an upcoming publication on the in vitro effects of UC2 materials. Considering the distribution of FLG material inside Epoxy-FLG, it is clear that abraded particles of respirable size are heterogeneous with respect to their contained amount of FLG.

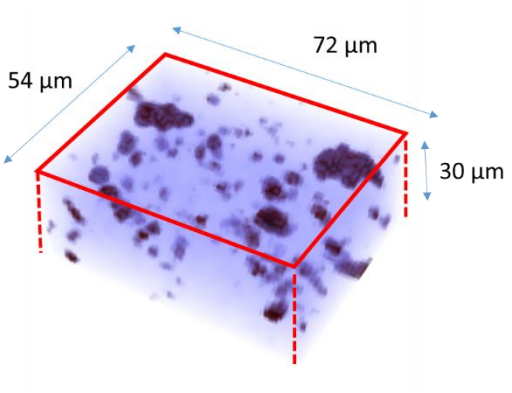


Figure 3: Three-dimensional reconstruction of the FLG distribution inside FLG-epoxy, the starting material of UC2. The confocal Raman image stack, prepared from 30 mappings taken down to a depth of 30 µm, reveals the heterogeneous size of the FLG, accounting for approximately 5% of the total mass.

2.4 UC2: Detection of Few Layer Graphene in Cells by Confocal Raman Microscopy

In the next step, abraded Epoxy-FLG, pure FLG, and the incinerated Epoxy-FLG were tested for their bioactivity in vitro using the Alveolar Macrophage Assay (AMA). One important result was that dispersed FLG induced a significant TNFα production in NR8383 macrophages. As such effects may be induced also via contacting receptor structures at the cell surface, it was necessary to confirm the uptake of all materials into cells by CRM.

Cytospin preparations of FLG-treated cells were examined by bright field and Raman microscopy. Light microscopy revealed heterogeneous assemblies of black material inside the cytoplasm which were identified by CRM as to be few layer graphene due to the occurrence of the D-, G- and 2D-Raman bands (Figure 3). Especially the sharp G-band at approximately 1580 cm^{-1} and the peak intensity ratios ID/IG and I2D/IG suggest that these inclusions were FLG rather than a compact structure such as graphite (c.f. Table 1).

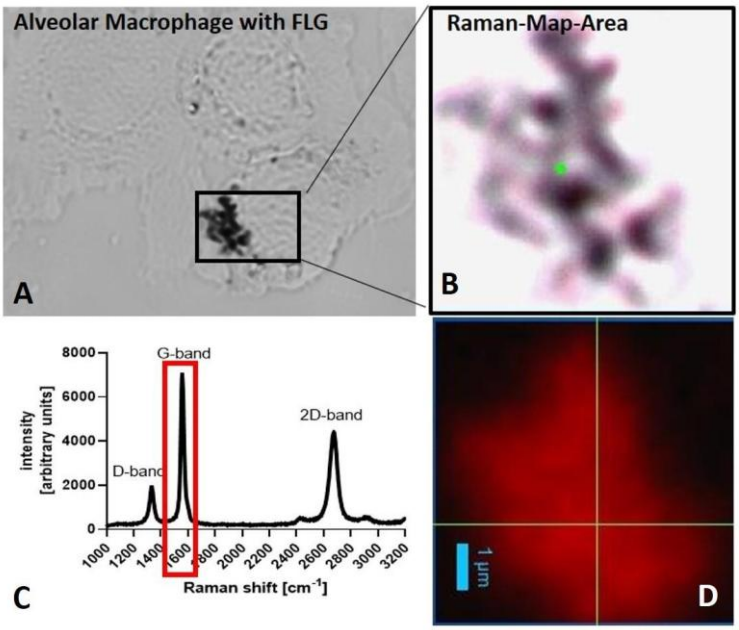


Figure 4: Results of the Confocal Raman Microscopy (CRM) of macrophages incubated with a dispersion of Few Layer Graphene (FLG) for 16 h. (A) Reflected light microscopy reveals various black inclusions in the cytoplasm outside the central, nuclear region. (B) Region selected from (A) for Raman mapping. (C) Raman spectrum with characteristic D-, G-, and 2D-bands Raman bands identifying the black material as FLG according to Table 1. (D) Raman mapping of the area in (B); the spatial distribution of the G-band, as highlighted in (C), is shown in red.

2.5 UC3: Detection and Characterisation of Graphene from Spray Material by Confocal Raman Microscopy

High-Resolution Imaging with CRM was also the method of choice to investigate the uptake of carbon materials included in UC3 materials, which consisted of five commercially available sprays meant to be used as surface protective agents or lubricants for cars and bicycles.

After several preliminary tests, the consortium agreed on using the spray "Graphene+Silicone" as an AdMa for further in vitro toxicity tests and uptake studies. Since the incubation of alveolar macrophages in the AMA is carried out under submerged conditions, preparing an aqueous dispersion was the major challenge. Silicone oils are clear, colourless, chemically inert, and, above all, hydrophobic liquids that cannot be dispersed in water. Numerous different dispersion protocols were tested, but a homogeneous, aqueous dispersion of the material was not achieved, mainly due to the inevitable separation of the silicone oil as an upper phase and the lower phase appearing as dark agglomerated material. Conventional testing in the AMA was, therefore, not possible. Since sprayed "Graphene+Silicone" was found to be respirable, a direct application of the spray onto human air-liquid interface (ALI) cell models was carried out. The uptake study under these conditions is still ongoing. Nevertheless, NR8383 macrophages were brought into contact with the dark graphene-containing material. To this end, and after phase separation of the above-mentioned dispersion, the upper hydrophobic phase containing the silicone oil was disregarded and the lower phase containing dark precipitates was mixed into cell culture medium and added to the macrophages. Bright field microscopic observations confirmed the presence of dark material in and between the cells and cytospin preparations of loaded macrophages were examined for the chemical nature of dark inclusions by Raman spectroscopy.

Figure 5 shows an inclusion of dark material in a cell. The Raman microscopic examination revealed characteristic bands, which allow the material to be identified as graphene-related, although the spectrum apparently pointed to more graphite-like structures. Electron microscopy of such an inclusion inside a cell showed lamellar as well as condensed structures underlining the interpretation that the material is in fact graphene-like.

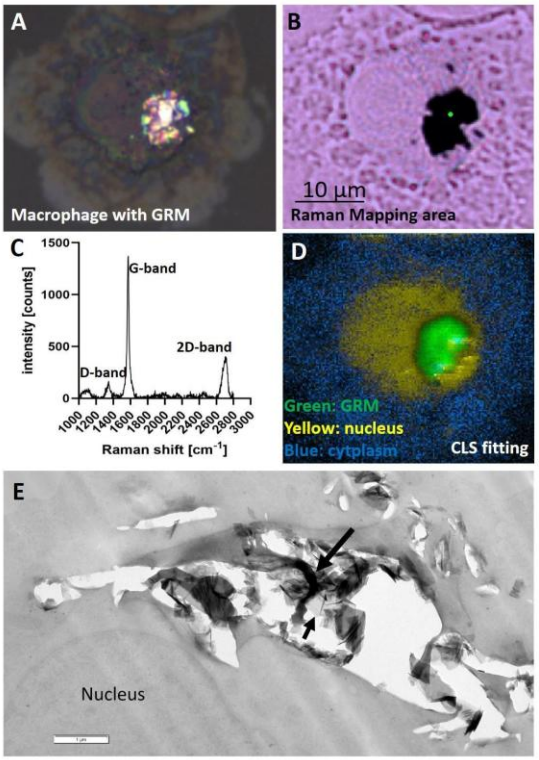


Figure 5: Results of Raman microscopy of a NR8383 macrophage incubated with the settled dark fraction prepared from UC3 Spray "Graphene+Silicone". (A) Darkfield and brightfield microscopy (B) show light scattering and dark material, respectively, seemingly located in the nuclear region, which had been artificially caused by centrifugation. Raman mapping reveals characteristic graphene-related bands (C). By CLS fitting (D) the spatial distribution of Raman bands corresponding to DNA (cell nucleus), cytoplasm, and GRM are displayed. E: Transmission electron microscopy image of a GRM-loaded NR8383 cell (Epon embedded, unstained 60 nm thick section). A large GRM agglomerate is seen in an electron-lucent, structureless area pointing to an artificial re-assembly after sectioning. The structure is located in the cytoplasm close to the nucleus; small and large arrows point to electron lucent and electron dense portions, respectively, representing different numbers of graphene layers.

To further characterise the black material, another UC3 spray designated as "100% Graphene Spray" was investigated. Spraying this material onto CaF carriers led to droplets of a greasy, oily material identified as to be paraffin by a typical Raman spectrum (Figure 6). Many of these droplets contained micron-sized black inclusions whose Raman bands pointed to graphite or few-layer graphene as a major component rather than graphene, due to the dominant G and the small 2D peak (Figure 6). However, due to the gradual differences in the banding pattern of all these components, the occurrence of minor amounts of graphene cannot be excluded. It is also noteworthy that the Raman spectra of the material in cells and on glass slides were highly congruent, showing that the sprayed GR2M material was engulfed by cells without being altered.

While CRM yielded qualitative results and confirmed the uptake of the material in question, quantitative data are hard to obtain by imaging. At least, the degree of cell loading can be

estimated for materials prone to gravitational settling and whose uptake can be inspected with light microscopic methods in combination with cytospin preparations.

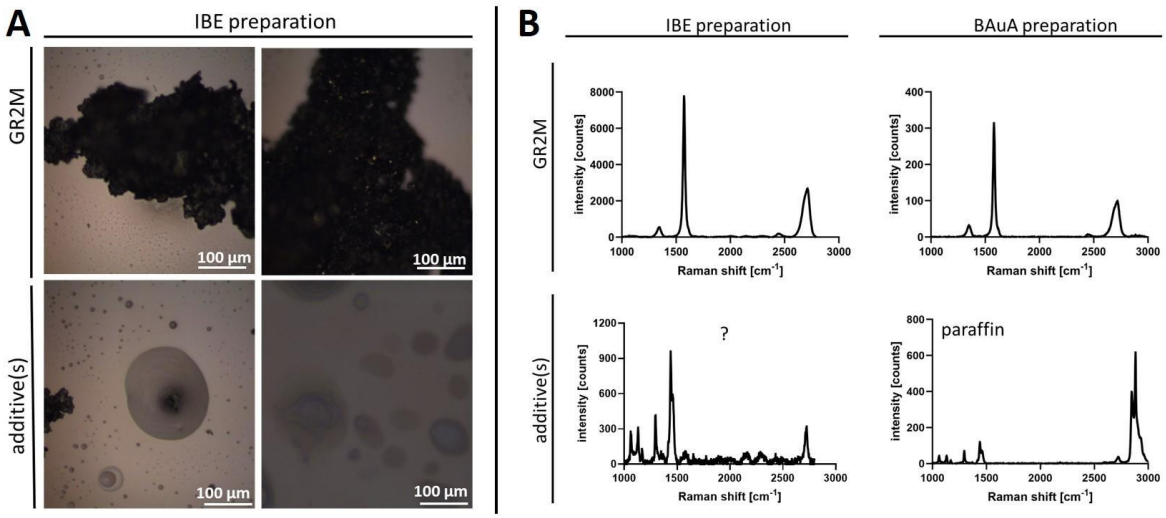


Figure 6: Comparative measurements of a "100% Graphene Spray" UC3 material with Raman microscopy at IBE and BAuA. (A) shows the sprayed material settled on CaF carriers which (upper, GR2M) contains large dark agglomerations of the graphene-related 2D material in question. The lower panels show oily drops (additive(s)) partially containing the dark material as well. (B) shows representative Raman spectra from the dark material (upper, GR2M) which was identified as graphene-related, and from the additive which was identified as to be paraffin by BAuA. Note that all spectra measured by IBE and BAuA were highly consistent.

2.6 Correlative Imaging of MWCNT NM-401 in NR8383 Cells by Confocal Raman Microscopy and Scanning Electron Microscopy

The previous sections have shown that CRM is suitable for detecting carbon materials in complex matrices like an epoxy matrix or in cells. In general, the main limitation of CRM for analysis of nanomaterials is due to the finite resolution of light microscopy used for 3Dl localisation[3], so that the term 'cell associated' may be preferable. To obtain more detailed pictures, a correlative imaging approach consisting of CRM followed by scanning electron microscopy (SEM) of the same scene was used by BAuA, allowing to combine chemical information and ultra high-resolution imaging. For this purpose, IBE supplied chemically fixed macrophages loaded with MWCNTs NM-401 on glass cover slips. The cells were critically point dried and investigated with CRM followed by SEM. Figure 7 shows an example in which a MWCNT fibre was chemically identified by its typical Raman signal. The corresponding SEM image shows the MWCNT fibre partly protruding from the cell, a phenomenon referred to as frustrated phagocytosis (FP), if in the end the cell is unable to fully ingest the fibre. Studying the dynamics of fibre uptake with time-lapse imaging may also help to decide as to whether a particular type of fibres elicits FP (see below).

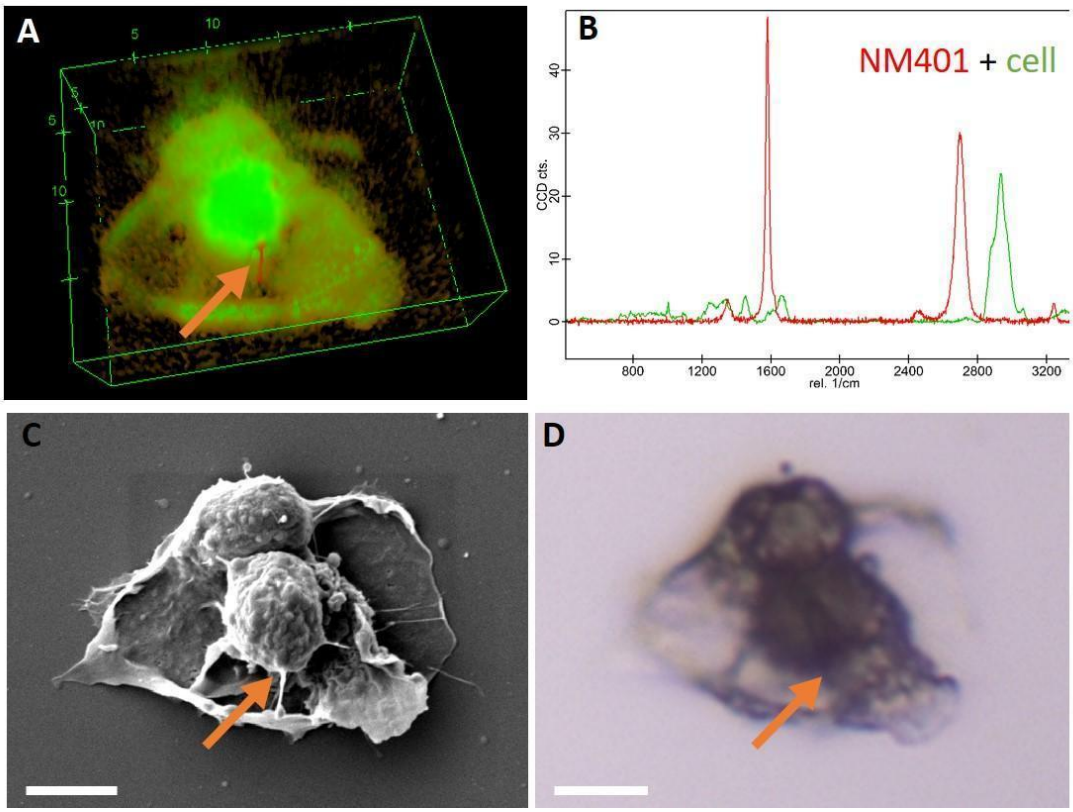


Figure 7: Correlative Imaging of a NR8383 macrophage treated with multiwalled carbon-nanotubes (MWCNT NM-401, 22.5 µg/ml). (A) 3D reconstruction of the Raman z-stack mapping showing the cell (green) and a multiwalled carbon-nanotube (red) protruding from the cell. (B) Corresponding Raman spectra with typical Raman bands of MWCNT NM-401 (red line) and cellular constituents (green line). (C) SEM image of the same cell found after automatically retracing the position. (D) Brightfield microscopy of the same cell (transmitted light mode); dark lines in the cell indicate MWCNT NM-401; arrows in (C) and (D) pointing at the same fibre structure. (Scale box in (A) in µm; all other scale bars show 5µm)

3 ToF-SIMS Analyses

ToF-SIMS methodology can be applied to biological tissue, e.g. to generate label-free, high-resolution images revealing the chemical and molecular composition of the tissue's near-surface region [4–6].

The operating principle of ToF-SIMS is based on the bombardment of the surface with primary ions, which induces the desorption of sample-specific secondary ions (secondary ion mass spectrometry, SIMS). These secondary ions can then be spatially resolved, separated according to their mass-to-charge ratio, and subsequently identified. Separation and detection are most frequently performed by a Time-of-Flight (ToF) detector[7].

In workpackage 2.1 ToF-SIMS was used for the characterisation of advanced materials for all use cases. Based on these results, ToF-SIMS investigations were carried out to explore the applicability of this powerful analytical imaging technique for the detection and characterisation of AdMas within a cellular surrounding. Alveolar macrophages (NR8383) were loaded with particulate material of respirable size down to nano-sized particles and used as a convenient cell model for the respiratory system.

Emphasis was put on the detection of graphene-related carbon materials of UC2 in comparison to carbon black and on the polymer-based PLGA particles from UC5. For carbon-based

materials, Raman Microscopy was employed as a benchmark technique as a first step. In the case of PLGA particles, fluorescence microscopy served this role. Wherever possible, these benchmark measurements were carried out on the same cell individual, thus enabling a direct and meaningful correlation.

3.1 Method Development for Correlative ToF-SIMS Measurements

The imaging of AdMa loaded cells using ToF-SIMS is still a rarely used approach and often needs special adaptations for unknown samples. In addition to the methodological challenges and instrumental settings for optimizing the measurement parameters, characteristic material-specific secondary ions need to be identified (Figure 8).

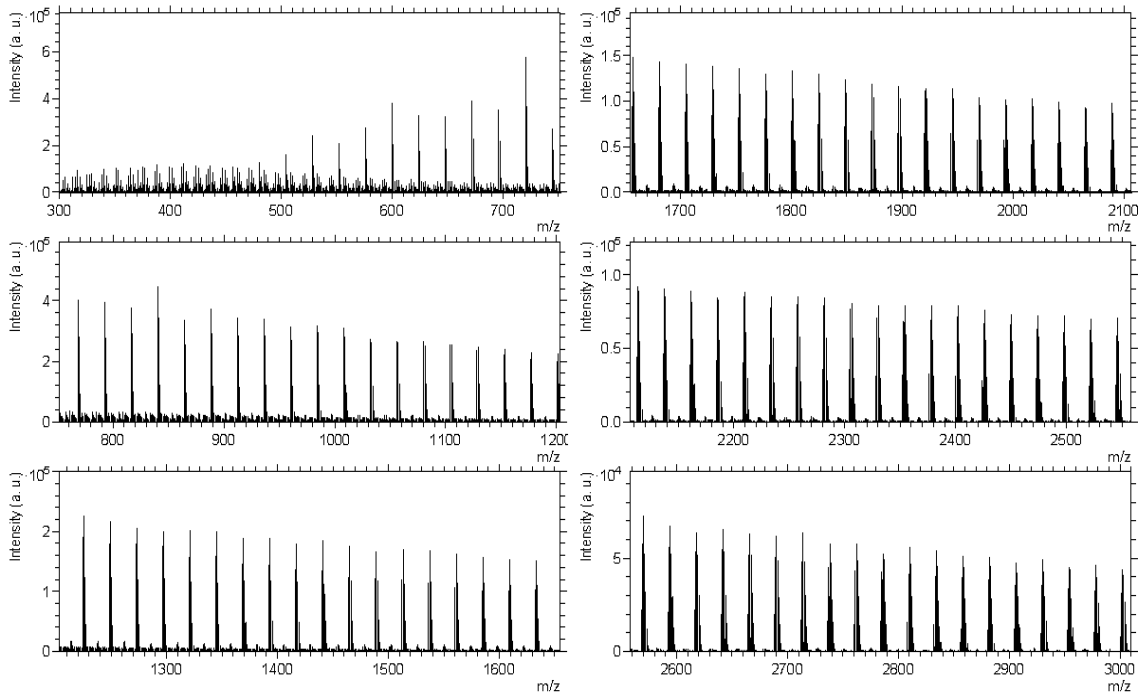


Figure 8: SIMS Spectra on pure graphene oxide material. Under the conditions shown here, numerous signals specific for graphene oxide were detected. Their typical composition is C_{2n}^+ while minor detergent contamination was detected. However, under the conditions optimised for cell imaging the number of signals are significantly decreased, e.g. as high mass components to not survive extensive primary ion bombardment that has to be used in SIMS-imaging.

ToF-SIMS is still a time-intensive technique and is therefore typically applied to small sample areas (e.g. 100 x 100 µm^2), although strategies to reduce the analysis time and to increase efficiency had been successfully implemented in the course of the project. Nevertheless, a preselection of suitable Regions of Interest (ROIs) followed by the transfer of the correct position to the ToF-SIMS instrument is necessary. Therefore, AdMa-loaded cells were seeded on gridded coverslips and viewed by either light, reflected light, fluorescence or Raman microscopy. Interesting grid positions were documented and transferred to the x-y-stage of the ToF-SIMS instrument, to achieve a correlative imaging. Because ToF-SIMS relies on the original chemical composition and eventually destroys the sample, the preceding microscopic examination method was carefully selected to have no or a negligible influence on sample chemistry. For carbon-based materials, CRM was employed as a benchmark technique in a first step. In the case of PLGA particles, fluorescence microscopy served this role. Wherever

possible, these benchmark measurements were carried out on the same cell individual, thus enabling a direct and meaningful comparison.

The method of how to transfer target cells from light microscopic inspection to ToF-SIMS analysis is exemplarily shown for inorganic Carbon Black (Figure 9). This material is easily detectable by light microscopy inside and also outside the cells due to the preparation by cytocentrifugation.

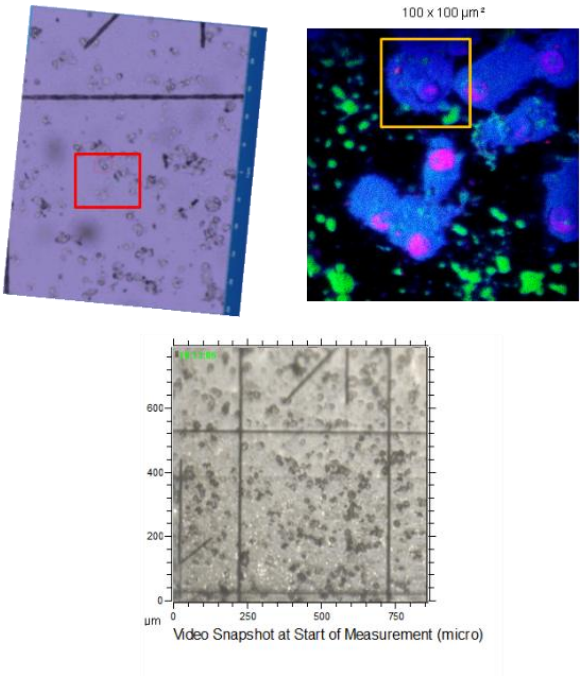


Figure 9: Comparison of a microscopic image (left), the image acquired with the camera of the ToF-SIMS instrument (bottom), and the ToF-SIMS image (right) of macrophages exposed to Carbon Black. In the ToF-SIMS image, carbon-specific signals are shown in green, phosphate signals in red, and the cell-specific CN^- signal in blue.

Figure 10 shows that Carbon Black which is seen as a black inclusion inside a cell by light microscopy, can be identified not only by Raman microscopy (left) but also by ToF-SIMS (right). The latter method may also add further information such as the phosphate distribution pointing to nuclear DNA. Overall, successful ToF-SIMS analysis of the target cell was achieved.

Thanks to these developments, successful ToF-SIMS analysis of the target cell was achieved. Moreover, contamination of the advanced material—specifically phosphate—could be detected within the cellular interior (Figure 10).

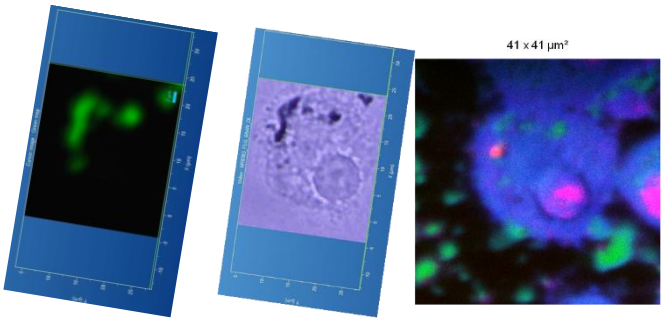


Figure 10: Comparison of images obtained by Raman microscopy (left), light microscopy (centre), and ToF-SIMS imaging (right) of the same individual macrophage loaded with Carbon Black. Carbon-specific signals are shown in green in both the Raman and ToF-SIMS images. In the ToF-SIMS image, the phosphate signal is displayed in red, while the cell-specific CN^- signal is shown in blue.

3.2 Detection of FLG by ToF-SIMS and Confocal Raman Microscopy

To detect FLG inside macrophages, the preparations were first measured using Raman spectroscopy, and individual cells were then measured using ToF-SIMS. Careful analysis of the spectral elements obtained from carbon enabled the intracellular detection of this carbon material based on chemical characteristics. Figure 11 shows that the FLG agglomerates visible as black inclusions in the bright field image correspond with the carbon-specific signals from the ToF-SIMS measurements. Other cell components such as the nucleus (detected as PO_2^- /PO_3^-) and cytoplasm (represented by CN^- signals from proteins) can also be visualised using this method allowing to allocate carbon-containing AdMas to cellular components.

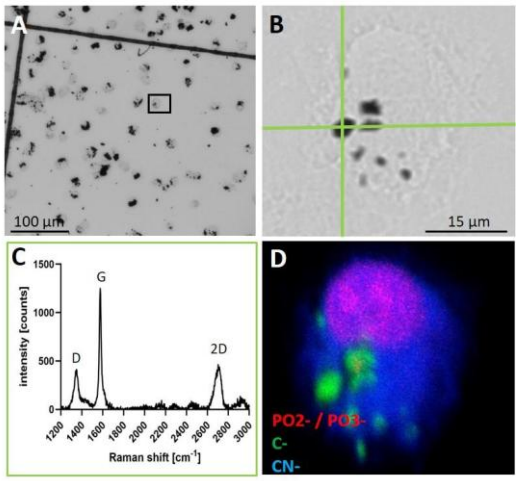


Figure 11: Correlative Raman and ToF-SIMS measurement of a FLG-loaded cell. (A) Bright field overview image of FLG-loaded NR8383 cells spun on a gridded coverslip with a cyto-centrifuge for Raman and ToF-SIMS measurements. (B) Higher magnification of the cell boxed in (A) showing several discrete dark spots; Laser position of the Raman measurement shown in (C) is indicated by the green cross. (C) Raman spectrum from the dark agglomerate marked in (B); characteristic D, G and 2D bands are typical for FLG. (D) ToF-SIMS imaging of the same macrophage; carbon-specific signals are shown in green, phosphate signal of the nucleus is displayed in red, and the protein-specific CN^- signal of the cell is shown in blue.

3.3 Correlative Imaging of PLGA in NR8383 Cells by ToF-SIMS and Fluorescence Microscopy

A benchmarking study comparing fluorescence microscopy and ToF-SIMS imaging was conducted using PLGA particles loaded with the fluorescent dye Lumogen[8,9]. Although emphasis was laid upon the detection of PLGA, the main drug-carrying AdMa of UC5, Secondary imaging Mass Spectroscopy (SIMS) followed by tandem mass spectrometry (MS/MS) allowed us to identify also the fluorophore and to extensively characterise its fragmentation pattern. MS/MS with an HCD (Higher-energy Collisional Dissociation) cell involves selecting a specific precursor ion in the mass spectrometer and fragmenting it by colliding it with an inert gas at high energy. The collision causes the precursor ion to break into smaller fragment ions, which are then analysed in a second stage of mass spectrometry. This process provides detailed structural information about the molecule.

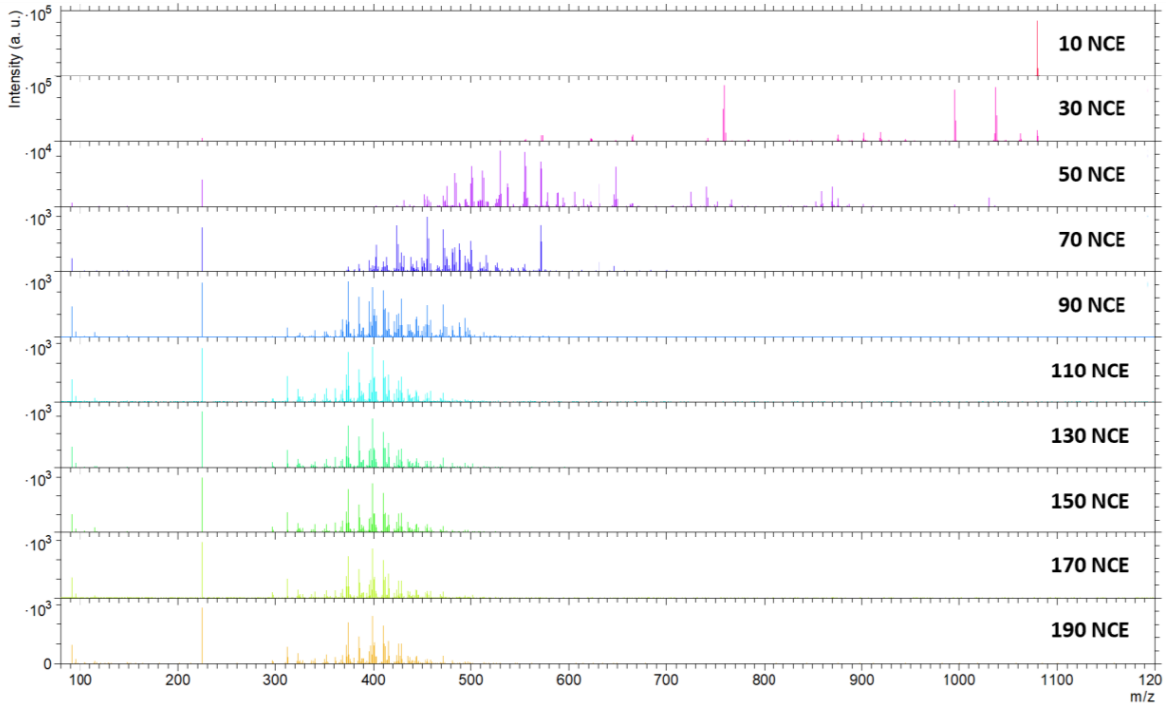


Figure 12: SIMS MS/MS fragmentation of Lumogen. This fluorphore was detected in PLGA particles and its fragmentation pattern was extensively studied under increasing Normalised Collision Energies (NCE): any detected signal is one fragment of the Lumogen molecule and the respective sum formula was assigned.

However, it turned out that the low concentration of Lumogen in cells incubated with Lumogen loaded PLGA-particles did not allow for the laterally resolved detection of this dye by ToF-SIMS, although fluorescence microscopy easily detected this fluorophore. However, ToF-SIMS was able to directly visualise the PLGA polymer matrix: Primary ion bombardment fragmented PLGA into a range of ion species, rendering this AdMa directly detectable by ToF-SIMS analysis. Thus, fluorescence microscopy, which is not able to detect PLGA, in combination with ToF-SISM could be applied in a correlative approach to describe both, the included fluorophore and the PLGA carrier.

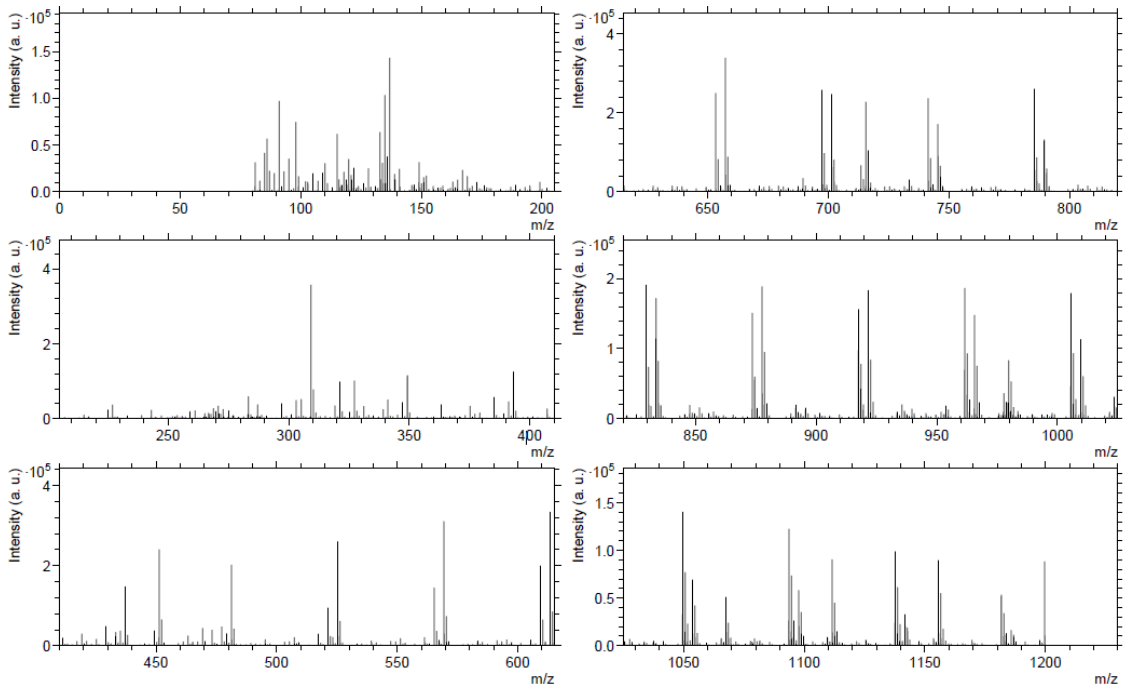


Figure 13: Lumogen containing PLGA particles analysed by Secondary Ion Mass Spectrometry. The analysis results in a comparatively complex but regular fragmentation pattern of the polymeric material. Beside polymer specific fragments also other materials like fatty acids and polysiloxane could be detected.

It turned out that this approach provided valuable insights into how Lumogen-loaded PLGA particles are metabolised by NR8383 alveolar macrophages.

This is illustrated in Figure 14 showing images of the cells incubated with Lumogen-loaded PLGA particles for 2 h (top) and 20 h (bottom). After 2 hours, both the fluorophore and the ToF-SIMS-detected PLGA show a similar distribution pattern and at least in some parts there was a co-localisation of Lumogen and PLGA as expected. After 20 hours, however, the fluorophore signal appeared either evenly distributed throughout the cytoplasm (whereby nuclear regions were spared) whereas in other cells it was confined to distinct vesicle-like intracellular regions which did not contain PLGA.

Overall, the combined analyses shed first light on the dynamics of PLGA handling by NR8383 cells. While PLGA remains concentrated in vesicle-like compartments over 20 h, the fluorophore appears to become released into the cytoplasm and may accumulate in secondary compartments (e.g. autophagosomes) different from the PLGA storing vesicles.

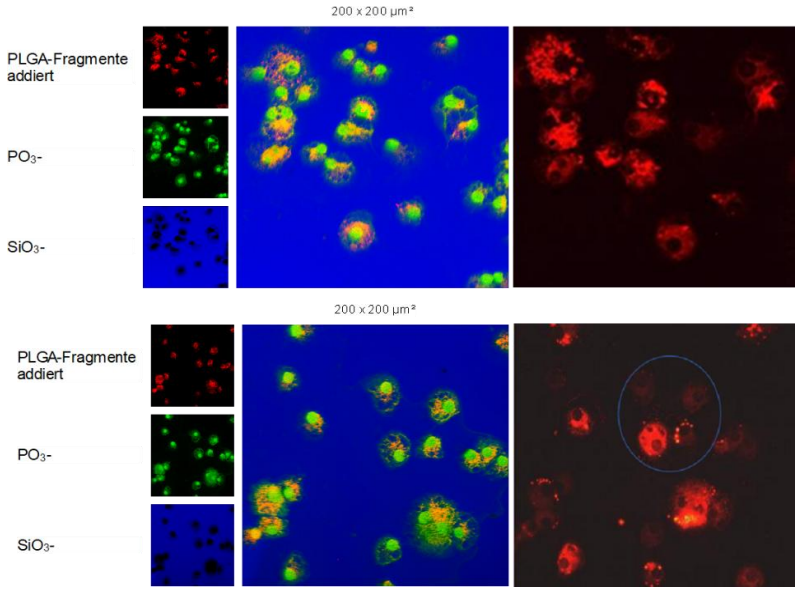


Figure 14: Comparison of ToF-SIMS imaging (left) and fluorescence microscopy (right) of macrophages exposed to PLGA particles loaded with the fluorophore Lumogen. Top row: After 2 hours of incubation, both the fluorophore (fluorescence microscopy) and the polymer (ToF-SIMS) show a similar, co-localised distribution. Bottom row: After 20 hours, the fluorophore signal is in some cells confined to specific intracellular regions (likely lysosomes), while the polymer remains widely distributed throughout the cell.

4 Time-Lapse Video Microscopy

A versatile approach to verify the uptake of materials into macrophages is time-lapse video microscopy. This technique allows capturing phase contrast or fluorescent images at predefined intervals so that the phagocytosis of microscopically visible particles or fibres can be documented while the cells move under cell culture conditions. Even under the non-confocal conditions usually applied for extended observations, particle uptake can be verified in a single optical plane, if the particle is clearly seen to be translocated inside the cell, or when the cell continues to move with its load. The technique is also highly useful to study the uptake of fibres, and/or to decide whether or not a fibre is subject to frustrated phagocytosis (FP), i.e., a state when macrophages are attached to fibres too long for complete ingestion[10,11]. Observations carried out by IBE and BAuA showed that not only the length of a fibre but also its flexural rigidity is important because thin, flexible fibres may be deformed by the macrophage and may allow complete ingestion (publication in preparation). Such a process may last more than 1 h and requires time-lapse video microscopy for documentation. It should be underlined that FP has been identified as a key event for lung cancer and mesothelioma. Therefore, a simple cell-based technique to distinguish - under biological conditions - rigid from flexible fibres is highly desirable.

Time-lapse videos were recorded for some selected materials using NR8383 cells, some of which were also used in the Alveolar Macrophage Assay (AMA). NR8383 cells are a cell line of lung alveolar macrophages which, as a component of the innate immune system, are specialised in taking up particles and fibres. Under culture conditions, NR8383 cells keep their motility which can pose a challenge on observations lasting for hours or even days. Limiting the number of cells per field of view and using reasonably low particle concentrations are key for successful time lapse recordings.

4.1 Time-Lapse Video Microscopy of NR8383 Cells with SiC and NM-401

Respirable Carbon nanotubes (CNTs) can be major constituents of AdMas, as exemplified by the materials of UC4 (CNTs in PU). Therefore, understanding the response of cells of the respiratory system is of utmost importance and part of Task 2.4 of WP2.

Silicon carbide (SiC) is a fibre and part of MACRAMÉ's control library. It is a long, inhalable nanofiber that is suspected of causing so-called frustrated phagocytosis in alveolar macrophages. This, in turn, leads to a persistent inflammatory reaction, which is considered a key event in the development of lung cancer. To better understand the phagocytosis process of this fibrous material, time-lapse video recordings were created. Figure 15 compiles individual video excerpts that illustrate that NR8383 cells attempt to ingest the fibres but have problems caused by the length of these obviously rigid fibres. It becomes clear from the images that many fibres are several times longer than the attached cells, and the macrophages are unable to shred, bend, or roll up the fibres, even over an extended period of time (in this case, 6 hours). This observation shows a typical example of frustrated phagocytosis and helps classify this material into this category. In a second example (Figure 16), we investigated NM-401 which is a multi-walled carbon nanotube (MWCNT). NM-401 was dispersed following the well-established NanoGenoTox protocol[12] which leads to a considerable amount of fibre-like agglomerates of seemingly critical dimension with respect to FP induction. Unlike SiC, and due to a variety of differently shaped NM-401 agglomerates, the uptake of NM-401 appears less instructive. However, the evaluation of the dynamic processes showing the interaction of the selected cell with several fibre bundles reveals that the cell is not capable of bending or coiling the fibre bundles so that it cannot completely ingest them. Therefore, this time-lapse video strongly suggests that NM-401, when dispersed this way, can indeed induce frustrated phagocytosis.

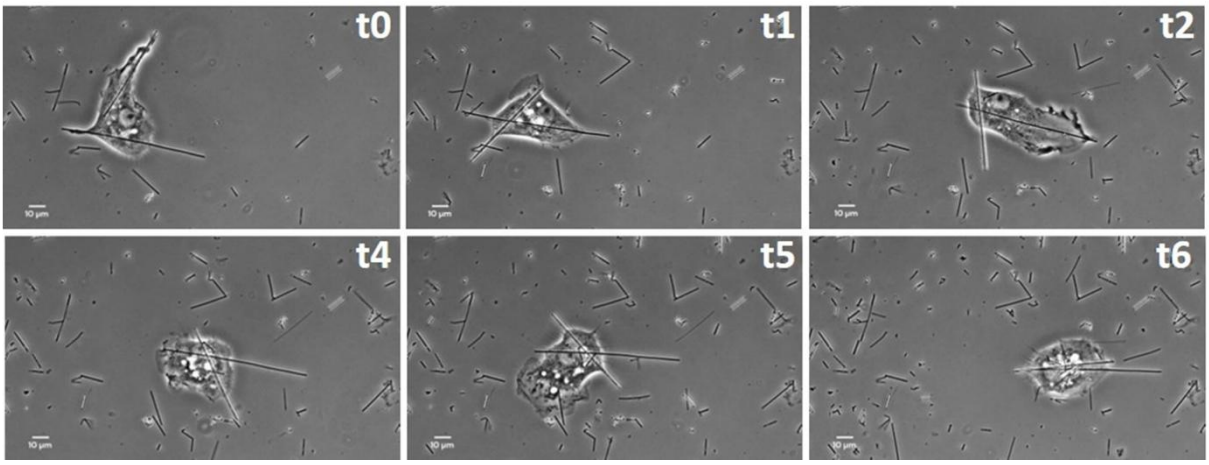


Figure 15: Time-Lapse Video Microscopy of a NR8383 alveolar macrophage in the process of frustrated phagocytosis with several SiC fibres. Indicated times t0 – t6 correspond to images taken up to 6 hours after fibres had been added to the culture.

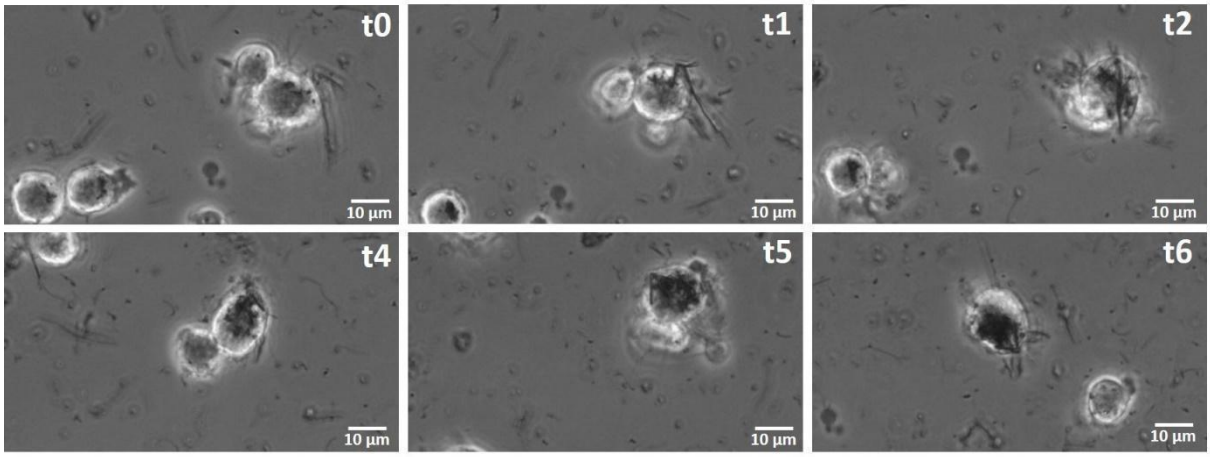


Figure 16: Time-Lapse Video Microscopy of NR8383 alveolar macrophages in contact with NM-401, a multiwalled carbon nanotube material. NM-401 was dispersed following the NanoGenotox protocol and administered with a concentration of 11.25 µg/mL. Indicated times t0 – t6 correspond to images taken up to 6 hours after fibres had been added to the culture. Unlike the situation with SiC (see Figure 15) the process here is less clear as only some fibre agglomerates are very long. However, successive images show that the cell is not capable of bending and/or completely ingesting the agglomerated fibre bundle, strongly suggesting that NM-401 at least in agglomerated form, gives rise to frustrated phagocytosis.

4.2 Time-Lapse Video Microscopy of NR8383 Cells with Graphene Oxide Material

Graphene oxide (GO) is part of MACRAMÉ's UC1. Although GO is generally believed to be easily dispersible, dispersion in serum-free F-12K medium, as used for NR8383 macrophages resulted in apparently large particles, whose compactness and uptake was questionable[13,14]. Using time lapse imaging the interaction of cells with particles was investigated. As seen in Figure 17, GO particles with a Feret diameter in the range of 20 µm were not ingested by the cells, which nevertheless contacted the particle surface. Data from the Alveolar Macrophage Assay showed an over-proportional release of the lytic enzyme glucuronidase, which often is a sign of attempted but unsuccessful phagocytosis, similar to what is occurring with fibres during FP. In the case of GO, time-lapse imaging was helpful to interpret this finding.

Unlike GO, the incinerated GO was fully ingested (Figure 18) and completely cleared from the bottom of the culture vessel.

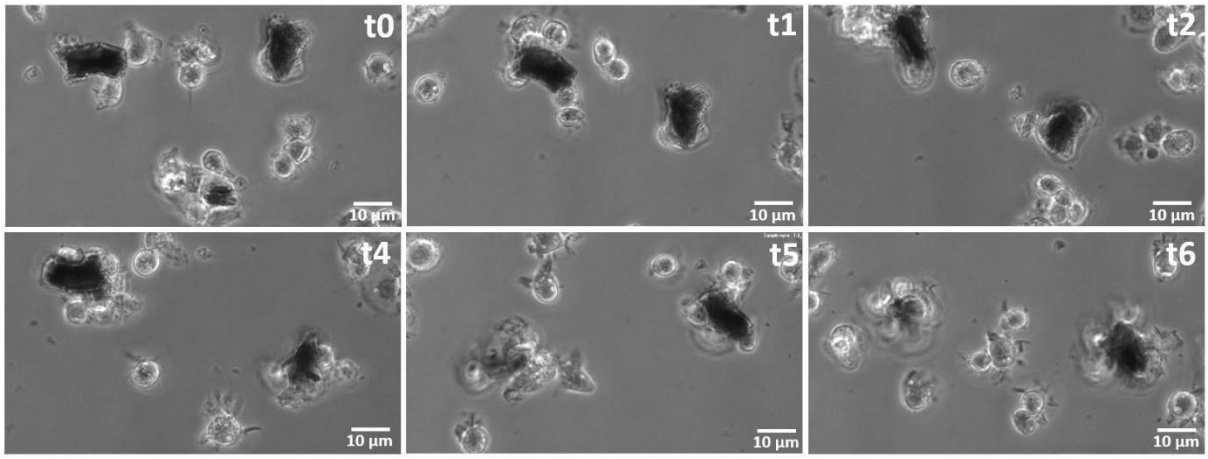


Figure 17: Time-Lapse Video Microscopy of NR8383 alveolar macrophages in contact with graphene oxide, dispersed following the Empa protocol (45 min water bath sonication) and administered with a concentration of 11.25 mg/mL. Indicated times t0 – t6 correspond to images taken up to 10 hours after fibres had been added to the culture. Cells were unable to ingest the large black particles (diameter approximately 20 µm) to which they appear to adhere.

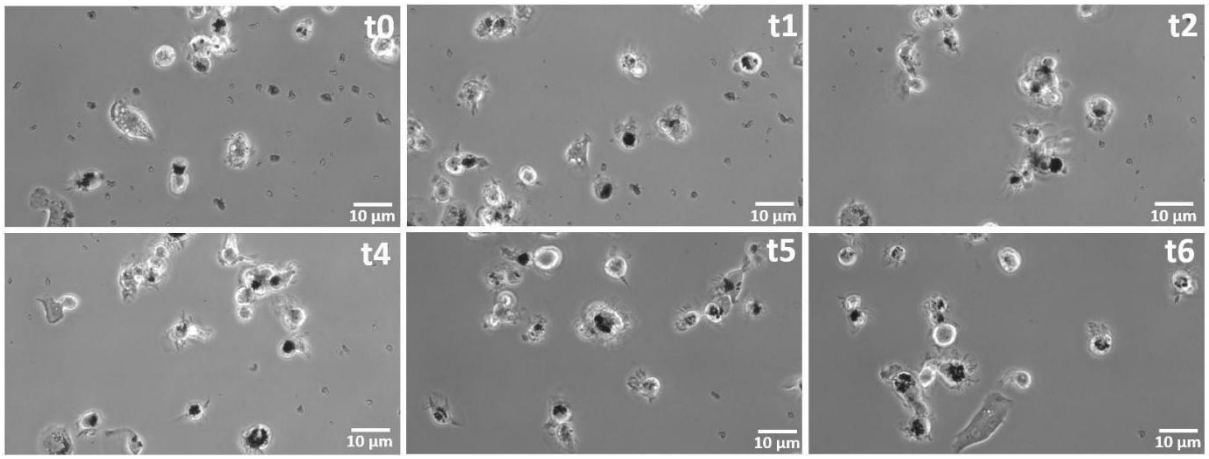


Figure 18: Time-Lapse Video Microscopy of NR8383 alveolar macrophages in contact with incinerated graphene oxide, dispersed following the Empa protocol (45 min water bath sonication) and administered with a concentration of 11.25 mg/mL. Indicated times t0 – t6 correspond to images taken up to 10 hours after fibres had been added to the culture. Cells were freely moving and ingested all soot particles, the largest of which were below 5 µm.

Overall, time-lapse-video microscopy is a versatile cell-based method not only to follow the uptake of particles and fibres but also to interpret findings of the macrophage assay. The method can be combined with fluorescent microscopy but is largely limited to submersed cultures of non-confluent cells. Although not a quantitative method, suitable software is capable to analyse image sequences and count the uptake of particles.

5 Enhanced Darkfield Microscopy

MACRAMÉ uses various in vitro models to investigate the effects of a wide range of materials on cells. Ensuring and observing the uptake of materials into single cells is of great interest but may pose a challenge. Many carbon-based materials appear as black materials under brightfield light microscopy and are easy to detect. However, non-fluorescent materials classified as nanomaterials due to a particle size of less than 100 nm cannot be detected by conventional light microscopy, but may be viewed by Enhanced Darkfield Microscopy (eDFM), a sophisticated type of darkfield microscopy using very intense white light which is guided by a fibre optics to a special oil-condenser. Images are taken with high resolution 40x or 100x (oil) immersion objectives and a numerical aperture of at least 1.0[15,16]. Strongly light scattering particles such as gold (Au) or silver(Ag)-based NP may appear as bright objects in different colours due to their size-dependent plasmonic resonance[17,18]. In MACRAMÉ the eDFM method was used for detecting PLGA-Au (from UC5) in cells and also to investigate the uptake of other materials some of which were not detectable by conventional light microscopy. Figure 19 shows a compilation of different materials in Papppenheim-stained NR8383 cells. While carbon-based materials such as graphene, SiC, and MWCNTs were visible as black materials, transparent silica-based materials such as SiO_2 NM-203 or DQ12 were visible by eDFM only. However, in the case of silica the Pappenheim-staining was mandatory because it left silica particles unstained while cell structures became blue and their light-scattering properties strongly reduced. Therefore, eDFM of Pappenheim-stained cytospin preparations was an ideal light microscopic method to visualise quartz DQ12 and also nano-sized amorphous silica particles such as SiO_2 NM-203. Because cells in cytospin preparations are very flat, the ingested particles and the major elements of the cells (cytoplasm, nucleus etc.) appear in one focal plane which allows for a semi-quantitative estimation of the particle content. In this respect, the method makes an important contribution to visualise the uptake of small particulates in cells.

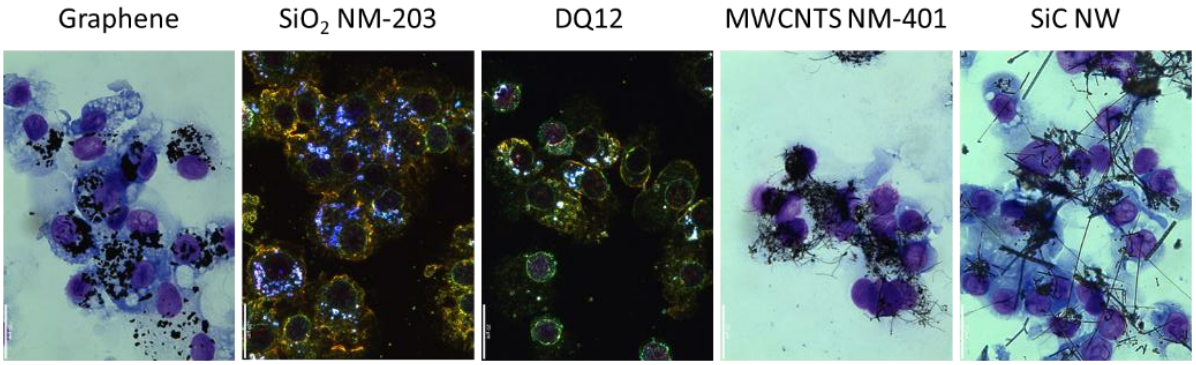


Figure 19: Brightfield (graphene, MWCNT NM-401, and SiC NW) and enhanced Darkfield Microscopy (SiO_2 NM-203, quartz DQ12) of Pappenheim-stained cytospin preparations of NR8383 cells. Note that the cells are differentially loaded with the material which relates to the LA-ICP-MS measurements of single cells (see above).

The Pappenheim staining approach was also advantageous to describe the uptake of materials from UC5 by eDFM. In order to obtain a real quantitative information about the uptake of PLGA, which was the main components of the organic AdMas representing UC5, MyBiotec provided 50 nm Au-doped PLGA particles, to indirectly measure the uptake of PLGA into cells by LA-ICP-MS using the Au signal. A particle size of 50 nm was chosen as it allows the detection of single Au-NP by both, LA-ICP-MS and eDFM. Figure 20 shows the Au-NP used for the labelling of PLGA in Pappenheim stained NR8383 cells. Unfortunately, the proportion of

Au/PLGA of the PLGA-Au particles turned out to be very low. Accordingly, PLGA-Au-treated cells showed pale inclusions, which were interpreted as to be PLGA as shown by the correlative fluorescence/ToF-SIMS study (see above). However, no typical Au-NP signals were found, a finding which was later on confirmed by electron microscopy (data not shown). Results suggest that the lack of the Au-signal in PLGA-Au treated cells could be overcome by increasing the Au/PLGA ratio of PLGA-Au.

Overall, eDFM in combination with conventional cell staining allows an easy and rapid semi-quantitative description of particle uptake. The method is primarily applicable to fixed cells on slides and coverslips, sections of tissue, and also to 3D cultures, as long as they are thin and the carriers do not profoundly disturb the light path.

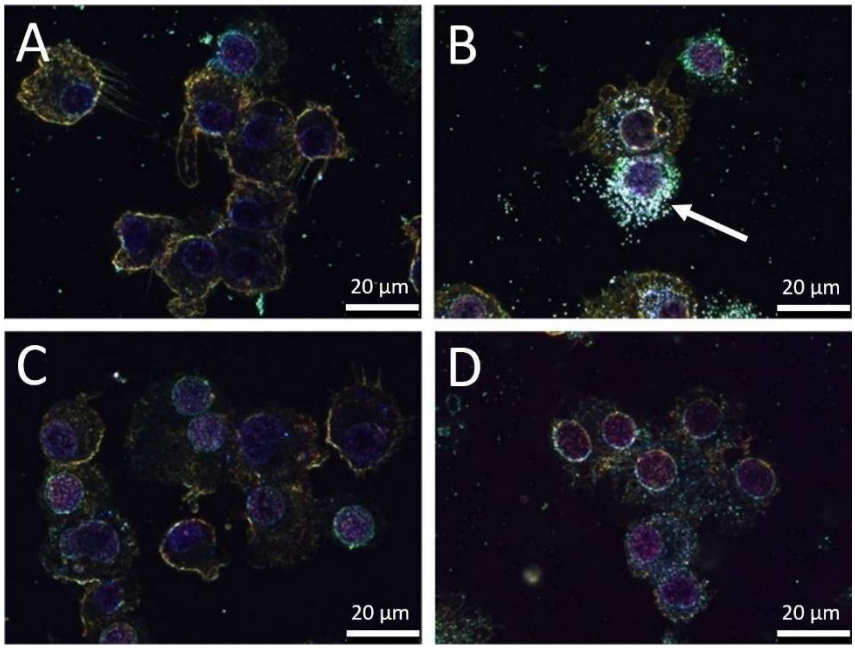


Figure 20: Enhanced Darkfield-Microscopy (eDFM) of NR8383 macrophages to analyse the uptake of Au-doped PLGA (UC5). Cytospin preparations of Pappenheim-stained cells. Gold-nanoparticle (Au-NP) used for PLGA labelling had a diameter of 50 nm. (A) control cells with few light scattering objects. (B) Cells loaded with 5 µg/mL of the original Au-NP (as used to prepare PLGA-Au); the arrow points to a heavily loaded cell with light scattering inclusions. (C) Same as (B) but with a concentration of only 0.05 µg/mL to match the gold concentration of the diluted PLGA preparation in D (calculation of concentration based on the PLGA-Au data sheet). Virtually no light-scattering Au-NP are seen inside cells. (D) Cells subjected to a non-toxic PLGA preparation (dilution factor: 500); the cytoplasm contains no bright but numerous pale bright inclusions, interpreted as PLGA containing endocytotic vesicles devoid of gold labelling. Since a higher concentration of PLGA-Au proofed to by cytotoxic no attempts were made to intensify the Au-PLGA loading for LA-ICP-MS investigation.

6 Quantitative LA-ICP-MS

Laser Ablation Inductively Coupled Plasma Mass Spectrometry (LA-ICP-MS) is an analytical technique used for the determination of the elemental composition of solid samples, like tissues[19–21]. In LA-ICP-MS, a high-powered laser beam is focused onto the surface of the sample, causing the material to be ablated. The ablated material is carried by a stream of inert gas, e.g., helium, into the inductively coupled plasma (ICP). In the plasma, the ablated material

is atomised and ionised. These ions are then introduced into the mass spectrometer, where they are separated based on their mass-to-charge ratio and detected with a mass spectrometer (MS)[22].

Aside from its advantages for solid sampling, LA-ICP-MS is most often used as an imaging technique as well, if the signal acquisition is performed in a time-resolved manner. After optimisation of the experimental settings combined with the time-resolved signal, LA-ICP-MS allows the creation of elemental maps (herein referred to as images) that offer spatial information about the composition of analysed samples. The acquired signal is distributed into pixels based on the laser scan speed (µm/s) and the integration time of the mass spectrometer (MS). Additionally, by utilizing the inherent quantification capabilities of ICP-MS, LA-ICP-MS provides quantitative information for the elemental distributions in a sample.

6.1 Method Development

In LA-ICP-MS, many parameters can be optimised and have influence on the data. The research in this work was focused on three parts: Assessment of quantification methods, suitable ablation techniques, and data evaluation methods. For all analyses, CytoSpin preparations of cells from the rat alveolar macrophage cell line NR8383 loaded with particles under defined conditions were used (supplied by IBE).

6.2 Quantification Method

Multiple methods for the quantitative analysis of sample contents have been described in the literature. Two possibly suitable methods for this study were compared: liquid calibration and calibration using microdroplet standards[23,24]. As a reference, isotope dilution analysis (IDA) was performed additionally. All experiments were conducted on the element Ce, because CeO_2 nanoparticles are one of the target analytes in this study.

(External) Liquid calibration is the standard quantification technique used in regular ICP-MS. Here, liquid standards of known concentration are introduced into the system and their signal intensity is measured. By performing linear regression, concentrations of unknown samples can be inferred via the resulting calibration line. For LA-ICP-MS, applying this technique is not trivial, as it requires a specialised introduction chamber which allows additional introduction of a liquid standard in addition to the laser ablation. However, once the system is in place, it is highly flexible to use in an elemental analysis laboratory because it only employs chemicals which are used on a day-to-day basis[23].

Another quantification strategy is to ablate microdroplets containing known absolute amounts of the target elements. The signal obtained from an individual droplet can in turn be related to the introduced mass of the target analyte, yielding quantitative information. This approach does not require additional instrumentation. However, the creation of new standards is cost- and time-intensive and can only be performed by laboratories with specialised equipment.[22,24]

Finally, the results were compared to a third method, isotope dilution analysis (IDA). IDA uses the naturally constant isotope distribution pattern of any given element. By spiking an isotopically enriched standard to a sample and comparing the isotope distribution in the sample to the expected ratio in the standard, the original concentration of the target element can be inferred. IDA is considered highly precise and compensates for losses during sample preparation and introduction. However, the high cost associated with the enriched standard rule it out for routine use, and it was therefore only used as a reference.[25,26]

All calibration methods were applied to a series of LA-ICP-MS analyses of NR8383 cells incubated with varying concentrations of CeO_2 NP. Cells were incubated with 0, 10, 30, 60 and 100 µg/mL CeO2. 100 cells were individually ablated, and the acquired signal was calibrated

with the respective methods. Resulting values are shown in Figure 21. No Ce signal was found in the blank, all other experiments did indicate cellular uptake of CeO_2 NP. Generally, liquid calibration and microdroplet calibration are in very good agreement, with relative deviations below 1% between all experiments (0.6%, 0.5%, 0.3%, 0.7% for 10, 30, 60, 100 µg/mL, respectively). Aside from the experiment with 10 µg/mL incubation concentration (0.2%, 0.4%), IDA calibration yields values between 14.9% and 17.1% lower than the other methods. Still, due to the high variance in individual intracellular concentrations, the results overall indicate applicability of both, liquid calibration and calibration with microdroplets. Due to the similarity of the results between liquid and microdroplets calibrations and the high availability of standards, the calibration with liquid introduction was used for subsequent experiments.

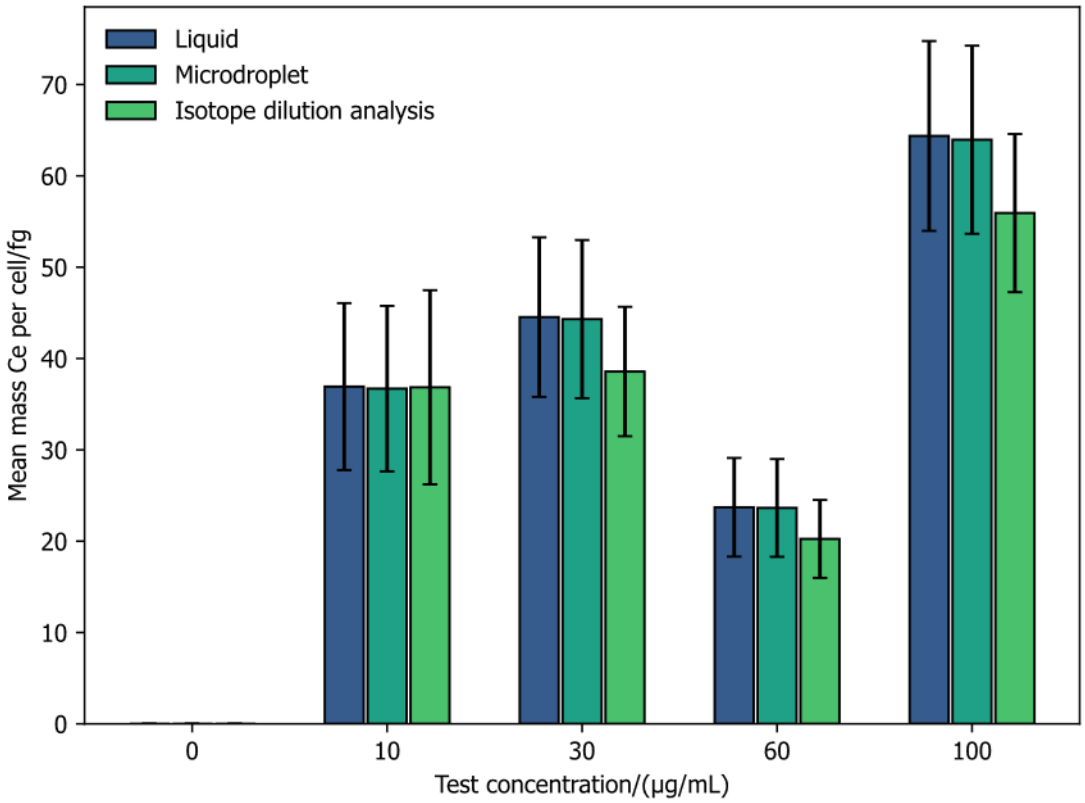


Figure 21: Results of calibration experiments. Mean intracellular Ce concentrations of n = 100 NR8383 cells incubated under varying conditions were determined using liquid, microdroplet, and IDA-based calibrations. Error bars indicate standard errors of the mean.

6.3 Ablation Techniques for Single-Cell LA-ICP-MS

LA-ICP-MS analysis offers two fundamentally different sampling approaches: Spot-by-spot and sequential ablation. Despite the imaging capabilities of LA-ICP-MS, this study on macrophages prepared on glass slides with a cytocentrifuge does not conceptually require spatially resolved images of cells. Spot-by-spot ablation would suffice to achieve single-cell information. Using this approach, per-cell elemental concentrations are determined by ablating individual cells in one shot with a large spot size and calibrating the resulting signal intensity (cf. Figure 22 a). While the method requires the manual selection of ablation spots, further data processing is straightforward. Therefore, the approach was considered viable and tested by ablating 100 individual NR8383 cells incubated with TiO_2 NM-105. The signal of 20/100 (20%) cells exceeded the maximum of the calibration range of 55,000 cts, which was not considered acceptable and therefore rendering this approach unusable for the experiments. Instead,

sequential ablation of the cells was considered. Here, a smaller spot size is used, and the samples get ablated line by line. By this the signal intensity of a cell is distributed over multiple pixels (cf. Figure 22 b) and highly intense signals overshooting the calibration range are avoided.

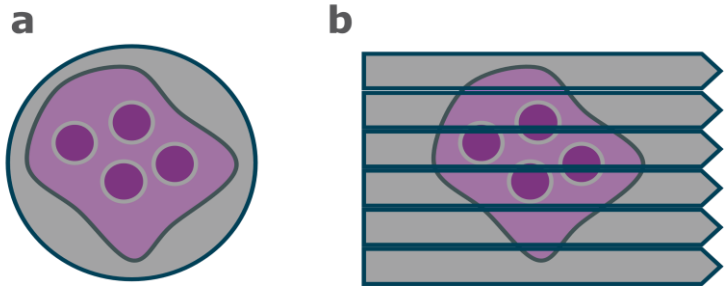


Figure 22: Schematic of different ablation modes. (a) One spot is used for the entire cell. (b) The cell is ablated line by line, distributing the signal over multiple pixels.

6.4 Data Evaluation

Selecting hundreds of cells from each image manually for data evaluation is not a viable approach, especially if large datasets are acquired or multiple different experiments are performed. Instead, an algorithm was developed to automatically identify and localise cells after generation of the elemental maps. The approach takes advantage of the multidimensionality of LA-ICP-MS data and involves the following 5 steps:

Simple approach:

1. Using phosphor (P) as a cell endogenous element, find all intensity values Ip where $I_p \geq 2 \cdot \text{Median}(I_p)$.
2. Eliminate all pixels from the set without immediate neighbours.
3. Find cell clusters by performing depth-first search (DFS) for each pixel that has not been attributed to a cluster.
4. Consider a cluster a cell, if it consists of at least five adjacent pixels.
5. Eliminate objects if they are larger than 40 µm×40 µm to avoid overlapping cells (this step is performed during further sample processing).

In addition to the simple approach, two potential improvements were also explored. The second algorithm features a geometry-based approach and fits a square around the maximum of the P cluster intensity. This deliberate overfitting is used to avoid target element underestimation if the NMs are located in low-P regions of cells.

Geometric approach:

6. Search maximum P intensity values in each cell cluster found in 3.
7. Using the respective target element, remove all maxima where $I_{te} \leq 2 \cdot \text{Mean}(I_{te})$; te: target element
8. Generate a square with size 40 µm×40 µm around the maximum and use the intensity found in these pixels for the determination of per-cell concentrations.

The third algorithm utilises the multidimensionality of LA-ICP-MS data: From the maximum intensity values in each cluster, an additional DFS is performed for each target element (verbose search). This approach should filter out all cells which did not take up enough NM to be distinguished from non-incubated cells. Additionally, if the P intensity and the Ce intensity hotspots are not completely congruent, the verbose approach should be able to correct the slight deviations.

Verbose approach:

6. Search maximum P intensity values in each cell cluster found in 3.
7. Using the respective target element, remove all maxima where

   $I_{te} \leq 2 \cdot \text{Mean}(I_{te})$; te: target element.

   Additionally, remove all pixels from the image map that do not fulfil this criterion.
8. Use the remaining maxima and pixels and perform DFS on the target element to find cell clusters according to 3. to 5.

Exemplary element maps of an experiment in which NR8383 cells had been incubated with Mn_2O_3 (22.5 µg/mL) is shown in Figure 23. The automatic fitting of cells conceptually works with all three approaches.

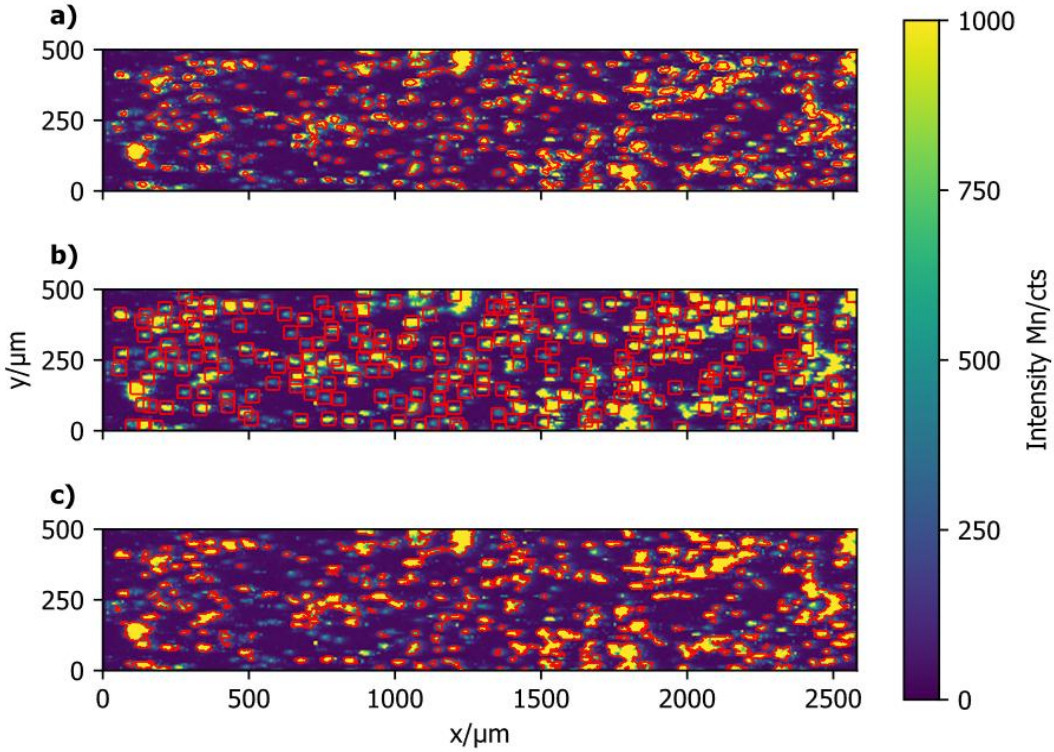


Figure 23: Visualisation of the three phosphorous-based cell recognition algorithms as used for automated evaluation. NR8383 cells were loaded with 22.5 µg/mL Mn_2O_3 for 16 h, detached from the cell culture well, suspended, and spin-dried onto a glass slide with a Cyto-centrifuge. The size of the scanned area was 500 µm x 2600 µm. Red lines indicate demarcate single cell regions as recognised by (a) the simple approach, (b) the geometric approach, and (c) the verbose approach.

Simple and verbose cell recognition show similar results, but the verbose approach indeed eliminated the expected under-fitting, if the hotspot locations slightly deviate. Overall, the geometric approach appeared to be most error-prone because the shape of the selected areas

did not represent the shape of cells, and led to stark overestimation and/or incorrect allocation of pixels in many cases (cf. Figure 24a, green circle). Compared to both other methods, the geometric approach also produced unreasonably large sizes per cell (Figure 24b). Therefore, the values obtained from this method were no longer considered.

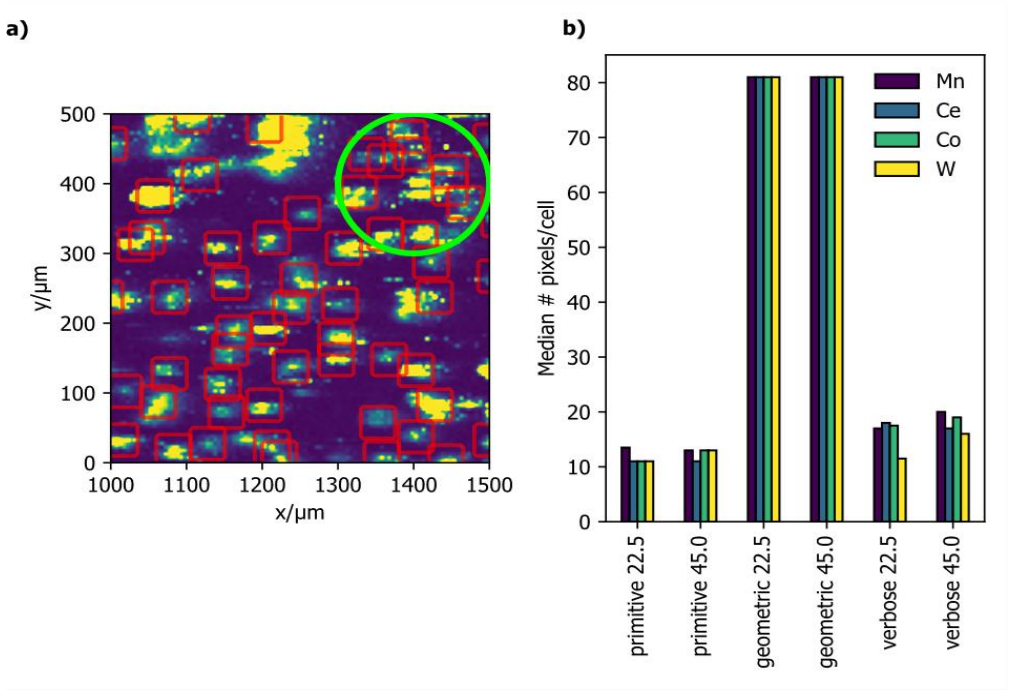


Figure 24: Flaws of the geometric approach. (a) Zoomed-in sector of Figure 18 showing inaccurate cell allocation. (b) Comparison of median pixel numbers "per cell" as obtained from the three approaches; data were taken from all experiments carried out to detect Mn, Ce, Co, and W (see experiments listed in Table 3).

6.5 Application of the Developed Automated Method

The LA-ICP-MS method as described in 1.5.4 was used to determine the NM uptake of individual macrophages in further incubation experiments. In total, six incubation experiments were conducted. The employed NM as well as their respective concentrations are listed in Table 3. In each experiment 100 cells were examined. From the applied dose (22.5 and 45 µg/mL in a volume of 200 µL), the number of cells seeded per well (3 x 10^5), and the optically controlled complete uptake of settled particles, a mean cellular uptake was calculated and amounted to 15,000 and 30,000 fg per cell, respectively.

Table 3: Particles and concentrations from MACRAMÉ's particle library as used for loading and preparation of NR8383 cells for LA-ICP-MS experiments.

NM	Name	Incubation concentration/(µg/mL)	
CeO_2 NM212	Cerium oxide	22.5	45.0
WC·Co	Tungsten carbide-cobalt	22.5	45.0
Mn_2O_3	Manganese oxide	22.5	45.0

Boxplots of per-cell concentrations obtained in each experiment are shown in Figure 25. The per-cell concentrations showed very broad, positively skewed, non-normal distributions in all experiments. Cellular uptake of NMs varied strongly and depended on the composition of the material. In general, CeO_2 NM212 was taken up most effectively, with median values reaching

up to 2013 fg/cell for the incubation at 45 µg/mL. Mn_2O_3 NPs were taken up second most. Here, the median concentration was determined to be 430 fg/cell. In contrast to the other NMs, WC-Co particles are taken up much less. The determined intracellular concentrations are one order of magnitude lower than both other materials, with W and Co taken up to a median concentration of 32 and 13 fg/cell, respectively, even at the highest incubation level.

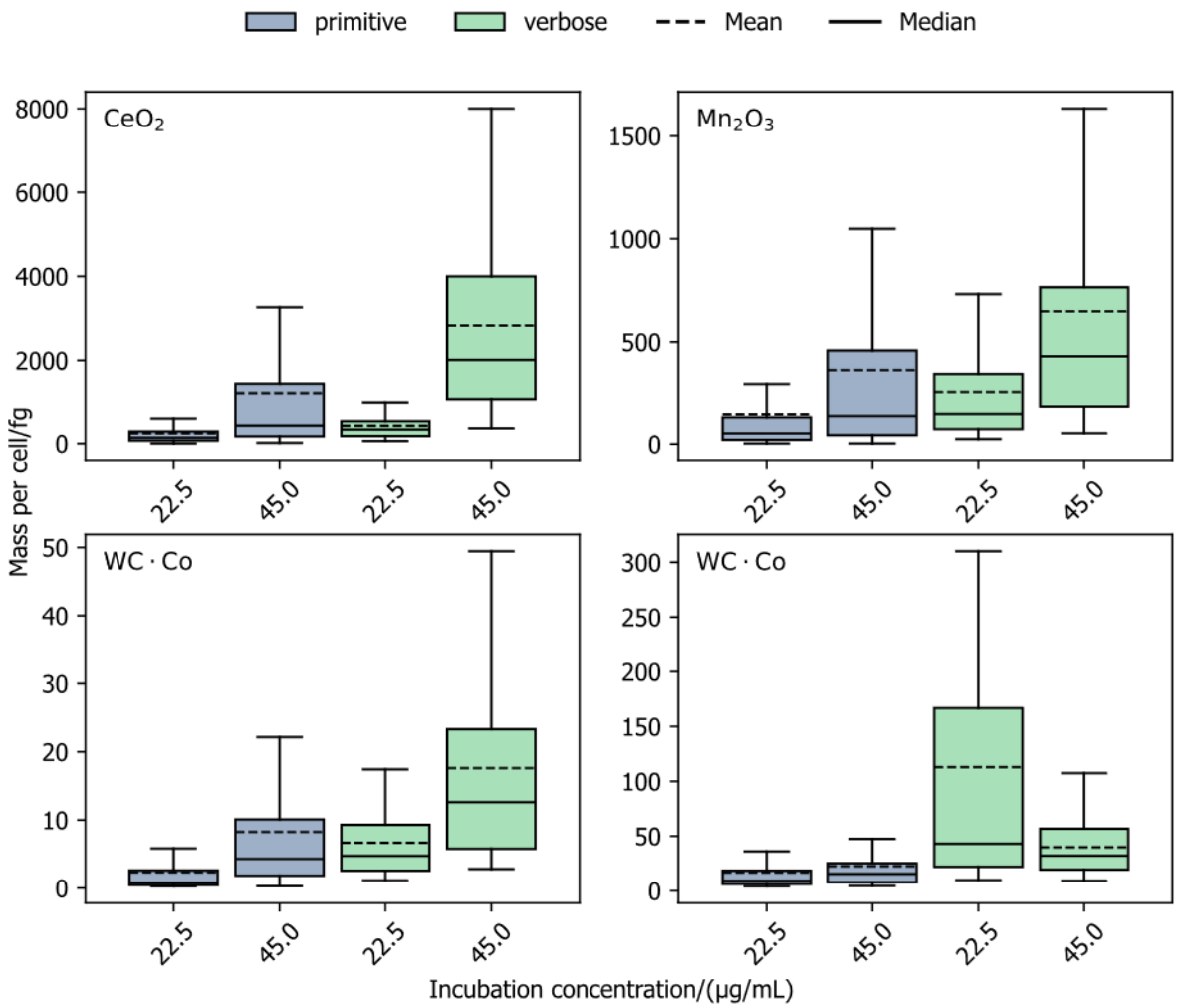


Figure 25: Boxplots of mass uptake distribution in all incubation experiments with different NMs determined with the optimised LA-ICP-MS method. Values after data evaluation with the simple (blue) and the verbose (green) algorithm of cell identification are shown. Median and mean values are indicated by a solid and a dashed line inside boxes, respectively. Boxes represent the range between 25th and 75th percentile (Q1/Q3), whiskers show Q1-1.5·IQR and Q3+1.5·IQR (interquartile range).

In general, the concentrations measured by LA-ICP-MS were significantly lower than expected from the well-established particle exposure of the alveolar macrophage assay, indicating that the method still requires some improvement. The high deviation could have various reasons, ranging from the incubation experiment itself to the analytical method.

Considering LA-ICP-MS, common measurement uncertainty sources include incomplete ablation, insufficient sample introduction, and calibration errors. However, the ablation efficiency of the LA was determined after every acquisition, and insufficient ablation was not observed for any sample. The potential errors coming from sample introduction efficiency can also be ruled out, as it was determined for each experiment and was considered in the

calibration to relate signal intensity to introduced mass. In addition, it can be assumed that a potential issue with the introduction efficiency would lead to uniform errors for all experiments due to the similar matrix of all samples.

It can also be ruled out that the concentrations were too high to be fully ingested, as particle uptake was optically controlled. It is well known that particle uptake by NR8383 cells is inhomogeneous (see also eDFM images above) with some cells ingesting high amounts of particles. Such overloaded cells tend to disintegrate and may not withstand the centrifugal force during cytospin preparation. Consequently, heavily loaded cells might have been disrupted and their load being released so that it was no longer attributable to the phosphorous signal by any of the methods. Such a mass bias or viability bias might then favour a deposition of cells which contained lower amounts of the respective NM. In fact, the overall counts of cell associated material showed that 25-76 percent of each analyte was cell associated, irrespective of the approach used for cell detection (data not shown), strongly suggesting that a considerable amount of material was released from the cells during the cytospin preparation. Future studies need to consider this bias and may prefer cells loaded with low, non-toxic amounts of particles.

Even without such a systematic error, a random selection error cannot be excluded. The broad distributions found in the cells indicate that large amounts of NP are taken up by only a few cells. Therefore, the sample size of 100 cells might have been non-representative to describe the general population. Here, longer measuring times could help improve the robustness of the descriptive statistics.

Despite these caveats, a new method for the quantitative analysis of NM uptake in single cells was developed by combining cytospin preparation with LA-ICP-MS and automated data processing. In the future, the method can be used to gain quantitative insights on the NM uptake in individual cells and can be used to study more NMs and cell types.

6.6 Quantitative Single Cell ICP-MS

Within MACRAMÉ, several tools were tested to characterise the advanced material toxicity at the cellular level. Among these, single cell ICP-MS (scICP-MS) was investigated as it has the potential to provide the quantification of internalised material/nanoparticles at the cell level, as long as they can be detected by ICP-MS. Therefore, within the project, scICP-MS was applied to gold-loaded cells only. Due to a delayed synthesis of the gold-labelled PLGA nanoparticles of UC5, as a first approach, the single cell ICP-MS method was applied to cells exposed to commercially available PVP-coated gold nanoparticles, which were considered most stable in suspension. For the investigation, the A549 cell line was selected as these cells are smaller than NR8383 macrophages making them more suitable for injection into the ICP-MS. Also, we expected a more even uptake of particles.

Samples were injected at a low flow rate (10 µL/min) into a high-efficiency sample introduction system (HE-SIS), following which they were analysed by inductively coupled plasma mass spectrometry (ICP-MS) for time resolved measurements of transient signals in millisecond intervals (5 ms). The transport efficiency (TE), i.e., the fraction of the particles from the suspensions that effectively reaches the plasma, was evaluated at up to 50 % for gold nanoparticles (Au-NPs) with a diameter of 100 nm. For smaller gold nanoparticles, the TE were in the same range. As an analogue to cells, we first investigated the transport efficiency for microplastic particles and found values of approximately 20 % and 1 % for 5 µm and 10 µm microplastics, respectively. Considering the size of A549 cells to be ≥ 10 µm, their transport efficiency was expected to be also low.

Control A549 cells and A549 cells loaded with commercial PVP-coated Au-NPs (50 nm) were prepared by IBE and analysed by single cell ICP-MS by LNE. Matrix-matching calibration was

performed since the cells were suspended in phosphate buffered saline (PBS). In addition to the analyte (Au) added in particulate form to the cells, iron (Fe) was used as a cell endogenous element to trace the cell number. Prior to analysis, the cell's integrity was checked with a microscope.

Iron analysis showed that no more than 0.2% of injected A549 cells reached the plasma. Gold analysis further indicated that the A549 cells were disrupted during injection, as a large peak largely congruent with that of the dispersed PVP-coated Au-NPs was observed for the Au-loaded A549 cells (Figure 26). However, this peak should not be present for the Au-loaded A549 cells, because (i) the control A549 cells did not contain any gold and (ii) the A549 cells loaded with PVP-coated Au-NPs were washed several times to remove any cell culture medium with extracellular Au particles before being re-suspended in PBS. Nevertheless, a loading of A549 cells with PVP-coated Au-NPs was estimated by considering only those data points larger than the peak, i.e. > 22 fg (see Figure 26). According to this diagram, single A549 cells may contain a broad range of PVP-coated Au-NPs, equivalent to a few dozen femtograms (fg) to a few hundred fg of gold (one PVP-coated Au-NP = 1.3 fg of gold). While this is a plausible result, it cannot be excluded that part of this initial estimation may also be associated with cellular debris together with complete cells.

Overall, the SC-ICP-MS analysis of the content of cells as large as 10 µm appears possible but still requires improvement of the injection part in order to minimise cell disruption and to ensure a constant, homogeneous and reproducible cell flow. When performing such measurements, special attention should also be paid to the medium matrices as we showed that PBS led to a high matrix effect shifting all gold intensities towards low values.

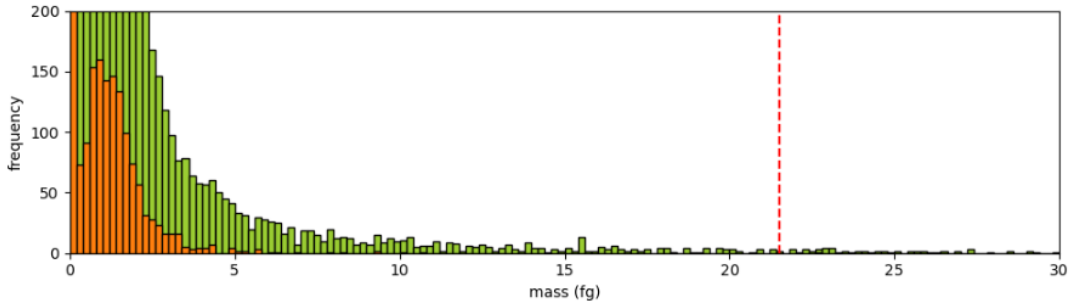


Figure 26: Gold mass distribution in PVP-coated Au-NPs suspended in PBS (in orange) and in A549 cells loaded with PVP-coated AuNPs (in green). The dashed line corresponds to the 99.9th percentile of PVP-coated Au-NPs suspended in PBS. Both samples were suspended in PBS.

7 Conclusions

Overall, the work carried out in this Deliverable has shown that a High-Resolution Imaging of AdMas in cell cultures is possible within certain limits, which are mainly set by the material. While dealing with several Use Cases, considerable progress has been made in detecting and identifying graphene-related materials in single cells and/or organic matrices. Confocal Raman Microscopy turned out to be the method of choice due to its spectral identification possibilities at high resolution, followed e.g. by ToF-SIMS which is another label-free method. However, light microscopic methods such as fluorescence and enhanced darkfield microscopy must not be overlooked as they were required to detect "inclusions" in cells and used to select regions of interest for the more sophisticated and time consuming imaging methods. In single cases, electron microscopy was necessary not only to study subcellular aspects such as particle uptake and compartmentalisation, but also to identify the type of particle by its morphology. The graphene spray provided with Use Case 3 provided an instructive example where ambiguous results required a combination of analytical methods eventually leading to conclusive results. It may be anticipated that this type of investigation is typical for the demanding task of identifying unknown AdMas in cells. Unlike the aforementioned methods, sc-ICP-MS and LA-ICP-MS were incorporated into the project as quantitative imaging methods, although they are not suited for carbonaceous materials. While the methods are well-established with respect to the use of standards necessary for a reliable quantification, we found it necessary to further explore the methods for transferring cells from cultures to the measurement set-up. While this was hardly successful for mammalian cells in case of sc-ICP-MS, the laser ablation approach together with a new, automated cell detection method worked well on cytospin preparations from dispersed cells dried onto glass carriers. We anticipate that also cells from complex 3D cultures, at least after enzymatic digest, can be subjected to this type of measurement. Therefore, this method to quantitatively describe the concentration of AdMas in different cell types appears universally applicable, and should be used in future studies.

8 Bibliography

1. Dieing, T. & Hollricher, O. High-resolution, high-speed confocal Raman imaging. *Vibrational Spectroscopy* **48**, 22–27 (2008).
2. National Physical Laboratory (NPL). Good Practice Guide No. 145: Characterisation of the Structure of Graphene. (2017).
3. Schmidt, R. *et al.* Correlative SEM-Raman microscopy to reveal nanoplastics in complex environments. *Micron* **144**, 103034 (2021).
4. Lockyer, N. Secondary ion mass spectrometry. *Nat Rev Methods Primers* **4**, 33 (2024).
5. Fletcher, J. S., Lockyer, N. P., Vaidyanathan, S. & Vickerman, J. C. TOF-SIMS 3D Biomolecular Imaging of *Xenopus laevis* Oocytes Using Buckminsterfullerene (C_{60}) Primary Ions. *Anal. Chem.* **79**, 2199–2206 (2007).
6. Breitenstein, D., Rommel, C. E., Möllers, R., Wegener, J. & Hagenhoff, B. The chemical composition of animal cells and their intracellular compartments reconstructed from 3D mass spectrometry. *Angew Chem Int Ed Engl* **46**, 5332–5335 (2007).
7. Fearn, S. *An Introduction to Time-Of-Flight Secondary Ion Mass Spectrometry (ToF-SIMS) and Its Application to Materials Science*. (Morgan & Claypool Publishers, San Rafael, 2015).
8. Juntke, J. *et al.* Testing of aerosolized ciprofloxacin nanocarriers on cystic fibrosis airway cells infected with P. aeruginosa biofilms. *Drug Deliv. and Transl. Res.* **11**, 1752–1765 (2021).
9. Günday, C. *et al.* Ciprofloxacin-loaded polymeric nanoparticles incorporated electrospun fibers for drug delivery in tissue engineering applications. *Drug Deliv. and Transl. Res.* **10**, 706–720 (2020).
10. Padmore, T., Stark, C., Turkevich, L. A. & Champion, J. A. Quantitative analysis of the role of fiber length on phagocytosis and inflammatory response by alveolar macrophages. *Biochimica et Biophysica Acta (BBA) - General Subjects* **1861**, 58–67 (2017).
11. Stobernack, T. *et al.* Predicting the morphology-driven pathogenicity of nanofibers through proteomic profiling. *Nano Today* **65**, 102812 (2025).
12. Rasmussen, K. *et al. Multi-Walled Carbon Nanotubes, NM-400, NM-401, NM-402, NM-403: Characterisation and Physico-Chemical Properties*. (Publications Office of the European Union, Luxembourg, 2014). doi:10.2788/10753.
13. Ma, J. *et al.* Crucial Role of Lateral Size for Graphene Oxide in Activating Macrophages and Stimulating Pro-inflammatory Responses in Cells and Animals. *ACS Nano* **9**, 10498–10515 (2015).
14. Lizonova, D., Trivanovic, U., Demokritou, P. & Kelesidis, G. A. Dispersion and Dosimetric Challenges of Hydrophobic Carbon-Based Nanoparticles in In Vitro Cellular Studies. *Nanomaterials* **14**, 589 (2024).
15. Vennemann, A., Alessandrini, F. & Wiemann, M. Differential Effects of Surface-Functionalized Zirconium Oxide Nanoparticles on Alveolar Macrophages, Rat Lung, and a Mouse Allergy Model. *Nanomaterials* **7**, 280 (2017).
16. Vennemann, A. *et al.* Subcellular detection of PEBCA particles in macrophages: combining darkfield microscopy, confocal Raman microscopy, and ToF–SIMS analysis. *Drug Deliv. and Transl. Res.* **12**, 2075–2088 (2022).
17. Vetten, M. A. *et al.* Label-free in vitro toxicity and uptake assessment of citrate stabilised gold nanoparticles in three cell lines. *Part Fibre Toxicol* **10**, 50 (2013).

18. Qian, W., Huang, X., Kang, B. & El-Sayed, M. A. Dark-field light scattering imaging of living cancer cell component from birth through division using bioconjugated gold nanoprobes. *J. Biomed. Opt.* **15**, 1 (2010).
19. Drescher, D. *et al.* Quantitative Imaging of Gold and Silver Nanoparticles in Single Eukaryotic Cells by Laser Ablation ICP-MS. *Anal. Chem.* **84**, 9684–9688 (2012).
20. Wang, M. *et al.* Quantitative Analysis of Gold Nanoparticles in Single Cells by Laser Ablation Inductively Coupled Plasma-Mass Spectrometry. *Anal. Chem.* **86**, 10252–10256 (2014).
21. Zheng, L.-N. *et al.* Determination of silver nanoparticles in single cells by microwell trapping and laser ablation ICP-MS determination. *J. Anal. At. Spectrom.* **34**, 915–921 (2019).
22. Seiffert, S. B. *et al.* LA-ICP-MS and Immunohistochemical Staining with Lanthanide-Labeled Antibodies to Study the Uptake of CeO_2 Nanoparticles by Macrophages in Tissue Sections. *Chem. Res. Toxicol.* **35**, 981–991 (2022).
23. Seiffert, S. B. *et al.* Calibration Strategy to Size and Localize Multi-Shaped Nanoparticles in Tissue Sections Using LA–spICP–MS. *Anal. Chem.* **95**, 6383–6390 (2023).
24. Schweikert, A. *et al.* Micro-droplet-based calibration for quantitative elemental bioimaging by LA-ICPMS. *Anal Bioanal Chem* **414**, 485–495 (2022).
25. Quinn, T. J. Primary methods of measurement and primary standards. *Metrologia* **34**, 61–65 (1997).
26. Clases, D., Gonzalez De Vega, R., Bishop, D. & Doble, P. SEC-ICP-MS and on-line isotope dilution analysis for characterisation and quantification of immunochemical assays. *Anal Bioanal Chem* **411**, 3553–3560 (2019).